Silicon Electrolyte Interface Stabilization (SEISta)

Quarter 1 report FY20

Anthony Burrell
National Renewable Energy Laboratory
15013 Denver West Parkway
Golden, CO 80401
Phone: (303) 384-6666
E-mail: anthony.burrell@nrel.gov

Brian Cunningham, DOE-EERE-VTO Program Manager
Hybrid Electric Systems, Battery R&D
Phone: (202) 586-8055
E-mail: brian.cunningham@ee.doe.gov

Table of Contents

Project Introduction

This report documents the Silicon Electrolyte Interface Stabilization team's approach in 1) characterizing the early-stage silicon solid-electrolyte interphase (SEI) including progress on identifying the specific reaction pathways present in the formation of the SEI layer, and 2) establishing a procedure for measuring SEI growth rate at fixed potentials and different cycling regimes.

Silicon is a viable alternative to graphitic carbon as an electrode in lithium-ion cells and can theoretically store >3,500 mAh/g. However, lifetime problems have been observed that severely limit its use in practical systems. The major issues appear to involve the stability of the electrolyte and the uncertainty associated with the formation of a stable SEI at the electrode. Recently, calendar-life studies have indicated that the SEI may not be stable even under conditions where the cell is supposedly static. Clearly, a more foundational understanding of the nature of the silicon/electrolyte interface is required if we are to solve these complex stability issues. A new multi-lab consortium has been formed to address a critical barrier in implementing a new class of materials used in lithium-ion batteries that will allow for smaller, cheaper, and better-performing batteries for electric-drive vehicles. This consortium, named the Silicon Electrolyte Interface Stabilization (SEISta) project, was formed to focus on overcoming the barrier to using such anode materials. Five national laboratories are involved: the National Renewable Energy Laboratory (NREL), Argonne National Laboratory (ANL), Lawrence Berkeley National Laboratory (LBNL), Oak Ridge National Laboratory (ORNL), and Sandia National Laboratories (SNL).

The SEISta project was specifically developed to tackle the foundational understanding of the formation and evolution of the solid-electrolyte interphase on silicon. This project will have as its primary goal an understanding of the reactivity of the silicon and lithiated silicon interface with the electrolyte in lithium-ion systems. It consists of researchers from NREL, ANL, LBNL, ORNL, and SNL working toward clear unified goals. The Silicon Deep-Dive team, which focuses on the science and technology barriers in functional electrodes, is a critical partner in this work. Many of the researchers are shared between both teams, and we hold joint meetings to ensure effective communication between the teams.

The current goals of SEISta are:

1. Have demonstrated ability to make model electrodes of Mg-Si zintl compounds and compared SEI chemistry to silicon using XPS, STEM-EDS and FTIR/Raman. **Q1 (100% complete)**
2. Have established experiments and protocols for understanding the factors that affect safety in silicon anodes, with a specific focus on highly exothermic reactions that occur at silicon electrodes. **Q1 (100% Complete)**
3. Have determined the affect that CO2 has on the stability of SEI formation on model electrodes, but examining the changes in the nature of the SEI (XPS, and FTIR/Raman and quantitate electrochemical measurement) as a function of CO2 concentration. **Q2**
4. Have determined zintl phase formation mechanism and its effect on SEI with model systems including Si NPs, Si wafer, a-Si thin film using XPS, AFM/SSRM, STEM-EDS and FTIR/Raman. **Q2**
5. **Go/NoGo** on production of tin-silicon alloys to be determined by the ability of the alloys to be prepared in 1g quantities and a demonstration that the alloys exhibit greater cyclic life than the pure metals alone. **Q2**
6. Have determined the chemistry and interfacial properties (e.g. nature of the chemical bonding at the surface of Si and the organic material) of LiPAA/Si interfaces as a function of charge (OCV, 0.8V, 0.4V, 0.15V, 0.05V) and drying temperature (100, 125, 150, 175, 200C). **Q3**

7. Have determined how binder changes the stress/strain on silicon electrodes as a function of state of charge by varying Si NP size and surface functionally utilizing both 2 or three dimensional model systems. **Q3**
8. Have implemented protocols that enable comparisons of safety responses in silicon anodes as a metric for improving safety in silicon cells. **Q3**
9. Have published a document that will enable other research and development groups to analyze stability of the SEI on a silicon-based anode, thus enabling developers or researchers to continually improve silicon cell stability (joint milestone with the Silicon Deep Dive). **Q4**
10. Have understood how the nature and amount of formed/soluble SEI species varies with electrolyte, binder, and Si anode (with surface functionalization) using GC-MS, (in-situ) FTIR/Raman and XPS. **Q4**

Approach

The SEISta team works to ensure that protocols for sample preparation, experimental design, and implementation as well as data reporting are consistent across the whole team. Each laboratory is working toward the same set of quarterly milestones using its own specific talents and capabilities in a concerted effort with the other team members. This joint focus results in multiple researchers interacting to produce and analyze data to ensure that individual experimental variations will not lead to erroneous results. Critical to the success of this effort is the use of standard samples that can be shared by all parties. In addition to weekly whole-team video presentations, we have held on-site face-to-face meetings each quarter for all team members and other interested parties to brainstorm and sort out issues with existing experiments and jointly develop new experimental plans.

Objectives

The critical issues that SEISta is attempting to address are:

What are the properties of the lithiated silicon/electrolyte interface?

What is the silicon SEI actually made of and what reactions are contributing to it?

How fast does the silicon SEI grow?

Does it stop growing?

Is it soluble?

Can it be stabilized?

For FY19, the team continues to focus on three broad tasks:

Materials Standardization—This task is critical to developing and deploying standardized samples and experimental procedures across the team. We will continue to provide full characterization to any new sample that is to be used for SEI studies to ensure reproducibility and full understanding of the material. This quarter's work focused on developing new oxide coatings and methods to control the thickness and density of oxide samples. In addition, work on the silicon nanoparticles has made progress with the enhancement of the materials collection and handling system in the plasma reactor. *Although this work dominated the early part of the project and is still critical to its success, it is now only a minor part of the work, and this is reflected in the relative balance of this quarterly report.*

Model Materials Development and Characterization—The nature of the electrode-electrolyte interaction in silicon electrodes is at the heart of the formation and stability of the SEI. The synthesis of well-defined silicon nanoparticles and the different chemical markups of lithiated silicon surfaces is being probed by preparing model compounds and thin films that may/can exist in silicon anodes. Lithium silicides, silicates, and other inorganic material (LiF, Li_2O) are being prepared, and their reactivity with electrolytes is being determined. These materials also act as standard spectroscopy samples for the researchers who are looking at the formation of the SEI on different silicon materials.

SEI Characterization—The overall objective for SEISta is to understand the nature and evolution of the SEI on silicon anodes. The materials standardization and model compounds will enable the researchers to systematically investigate the formation of the solid-electrode interphase using a wide variety of spectroscopy techniques—from different optical, microscopy, and electrochemistry—to determine how the SEI forms based on the nature of the silicon surface, and how it evolves over time. This section of work will continue to grow in scope as we move beyond the sample-characterization phase of the project and toward understanding the nature and evolution of the SEI. *This part of the project now represents the bulk of the work and, as such, this quarterly report is largely reporting on work leading to this outcome*.

Part 1: Understanding the thermal evolution of the SEI

Science of Safety: Temperature Dependent Reactivity of Silicon Anodes in Electrolyte (Q1 Milestone)

Bertrand Tremolet de Villers, Yeyoung Ha, Zhifei Li, Sang-Don Han, and Matthew Keyser

Background

The 2025 U.S. Department of Energy's (DOE's) battery goals of anode capacity of greater than 1000 mAh/g, $100/kWh pack cost, and fast charge of 20-80% SOC in 15 minutes require battery packs that have higher energy densities, resulting in a very compact system. To meet the specific energy goal, the electrode thickness of the battery will need to increase while decreasing the thickness of the current collectors. Furthermore, the amount of electrochemically inactive material, such as binders, will need to decrease. All of these factors will have a deleterious effect on the electrochemical and thermal performance of the cell. Furthermore, many of the advanced chemistries being developed to attain these goals, such as silicon and lithium metal anodes along with high-energy cathodes, have heretofore suffered from low efficiencies at low to moderate charge and discharge rates and have shown issues with lithium plating. Over the past year, NREL has led the SEIsta program in order to make silicon systems viable for vehicle technologies. In parallel to this effort, we need to understand the fundamental safety issues of silicon systems - previous work has shown that silicon systems are more reactive than their graphite counterparts.

Results - Path Forward

Cell Test Procedure:

Under this effort, NREL is investigating silicon thin film cells to understand the underlying thermodynamics associated with SEI instability. NREL has set up a facility capable of performing in-situ Raman and IR spectrographic analysis of silicon thin film samples as a function of temperature. The resulting gases from the thermal events can be evaluated using a Gas Chromatography – Mass Spectrometry (GC-MS). The goal of our experiments is to understand how the SEI changes as it morphs from a stable state to where decomposition begins. The data collected with the NREL testing will be analyzed alongside data collected using static and in-situ cells in other parts of the SEISta projects (LBNL, ORNL, NREL). NREL will use the data garnered from these experiments, coupled with theory insights from UC-Berkley, to inform our silicon abuse battery models which will be used to predict new electrolyte and additive combinations to lessen the severity of the thermal runaway event and eventually stabilize the SEI on silicon.

Past experiments with lithium-ion chemistries have shown that by analyzing the voltage signal and controlling the trigger heat to the sample allows for the necessary time to use Raman and IR to understand the chemical and morphological changes of the SEI layer. Figure 1 shows how the cell experiences a voltage sag right before the cell goes into thermal runaway. As long as the temperature/temperature rise are controlled, we should have enough delay to characterize the changes within the SiEI using SERS, XPS, and GC-MS before the cell enters into thermal runaway.

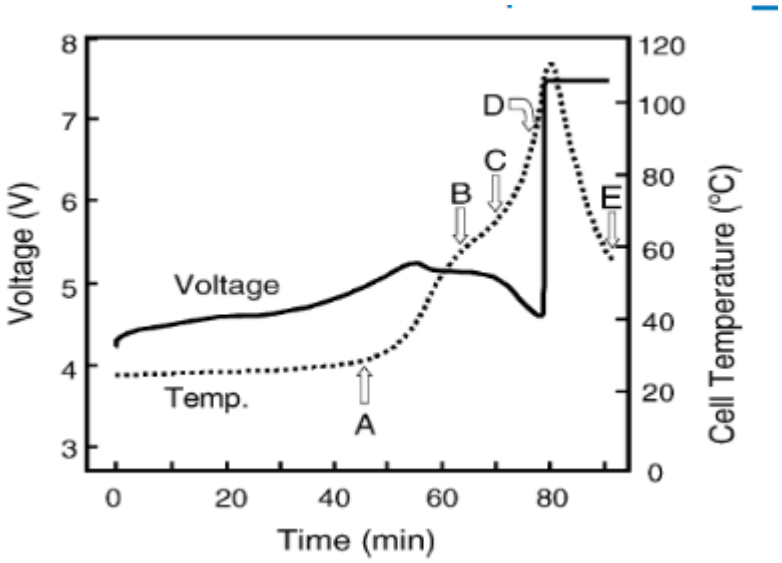

Figure 1. Voltage profile as cell enters thermal runaway.

Test Apparatus:

NREL modified a commercial cell to simultaneously allow micro-Raman measurements of a-Si on copper mesh anode. The cell will allow for temperature control and the ability to electrochemically cycle the battery. The spectroelectrochemical cell (ECC-Opto-Std, EL-CELL) has been modified by adding a metal ceramic heater and temperature sensing thermocouple. A dual channel potentiostat/galvanostat (Biologic-SP300) is used to control battery cycling and the heater current (cell temperature). The temperature range of this test setup is room temperature to approximately 100°C. The test setup and sample results are shown in Figure 2.

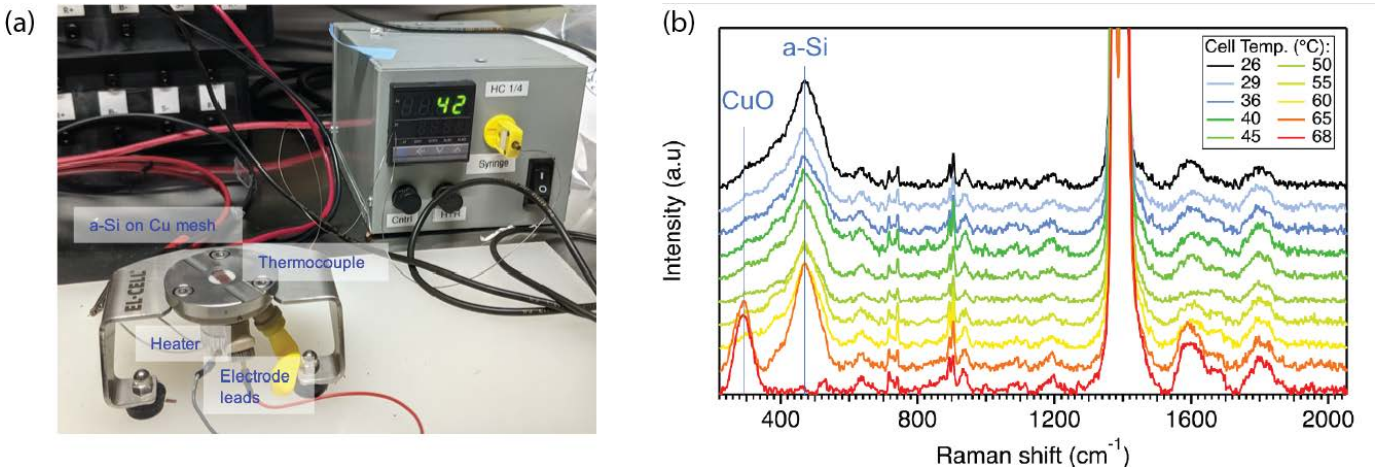

Figure 2. a) In-situ Raman cell modified for elevated temperature studies with a heater, temperature sensor, and exhaust gas. (b) Temperature dependent SERS spectra of an a-Si/Li half-cell at OCV in $LiPF_6$-based electrolyte.

We are also investigating a custom coin cell setup to run our experiments. The previously described EL-CELL is flooded with electrolyte during usage and as the temperature of the cell increases, we have noted issues with boiling electrolyte. Thus, to minimize the electrolyte volume required, we are designing a coin cell rig that allows for the same environmental and cycling conditions ("operando" rather than "in situ"). With the coin cell setup, we use a Linkam Stage for the precise temperature control. We are designing the windowed cell in

collaboration with Sandia National Laboratory - Josey McBrayer and Chris Apblett. The coin cell has a 2 mm diameter hole in the top of the cell covered with a sapphire window. Currently we are optimizing the cell configuration and the stage setup, such as how to attach the window to the coin cell cap, what electrode configurations to use, and how to mount the cell on the spectrometer stage, to get stable electrochemical and spectroscopic signals.

Anode/cell Studies:

In order to study the Si anode behavior at elevated temperatures, we first plan to mimic the conditions in a lithium half-cell configuration that we heat up to approximately 100°C. The working electrode was fabricated by sputtering 30 nm of Si onto both sides of a Cu mesh (#100). Before deposition of a-Si, we electrochemically roughened the copper mesh, creating a nanostructured electrode that enables surface-enhanced Raman scattering (SERS), a technique we recently developed and used to monitor the spectral evolution of silicon anode and associated SiEI during electrochemical cycling.[1] A Li metal foil was used as both the counter and reference electrode. The electrodes were assembled in a sandwich type configuration (Si/glass fiber separator/Li) and 100μL of electrolyte was added (either 1.2M $LiPF_6$ or 1.2m LiTFSI, in ethylene carbonate (EC):ethyl methyl carbonate (EMC) [3:7 wt:wt]). The cell was assembled in an Ar-filled glove box. We have observed charging/discharging behavior similar to that achieved with this system in a standard 2032 "coin-cell".

Once the half-cell configuration is optimized, we will proceed with a composite electrode as initial studies showed varied results from the thin film electrode. The next steps will involve moving towards using the composite electrode for in-situ SERS. One obstacle is the coating has to be thin (30 nm or less) to have the SERS effect. We are planning on varying different parameters, such as the concentration of the active material in the slurry and coating method to fabricate the composite electrode suitable for the SERS measurements.

To understand the true performance of Si at different temperatures, we are testing/proposing three different types of cell configurations: (1) Si/Li half-cells; (2) Si/NMC532 full-cells; and (3) Si/Li_xSi symmetric cells. All of these cell types will be investigated during our study.

Electrolyte Studies:

The initial electrolyte work is focusing on $LiPF_6$- and TFSI- in EC:EMC [3:7 wt: wt]. For the initial $LiPF_6$ study, we tested our cell design by assembling the half-cell components, then heating the cell while monitoring the open-circuit voltage and measuring the SERS. Figure 2b shows the temperature dependent SERS spectra. Between 65°C and 70°C, the a-Si peak centered at 470cm^{-1} disappears, and instead a peak emerges at 292cm^{-1} that is attributed to the CuO from the current collector.[2] No other significant spectral changes are observed. This suggests that in the presence of $LiPF_6$ at elevated temperatures, the a-Si thin film is removed from the copper mesh substrate. Note that the large peaks between 1300 and 1500cm^{-1} are from the sapphire window of the cell. Most other peaks originate from the electrolyte components. Electrochemical cycling was not possible at 70 °C with the $LiPF_6$-based electrolyte.

Figure 3a shows a photograph of the degraded Si on Cu mesh electrode inside the spectroelectrochemical cell after heating to 70°C. A fresh anode is also shown for comparison. It is clear that the Si anode has reacted and potentially dissolved in the heated electrolyte. It is our hypothesis that $LiPF_6$ and a-Si may be incompatible at temperatures greater than 65°C, as shown in the reaction scheme below. In carbonate-based solvents, $LiPF_6$ is known to dissociate into LiF and PF_5. The hydrolysis of PF_5 (with trace amounts of water) yields HF in solution. Hydrofluoric acid reacts with Si yielding SiF_4 and hydrogen gases. HF will also etch any SiO_2 present, leading to the formation of more H_2O that can continue the hydrolysis of PF_5. These reactions are likely accelerated at elevated temperature.

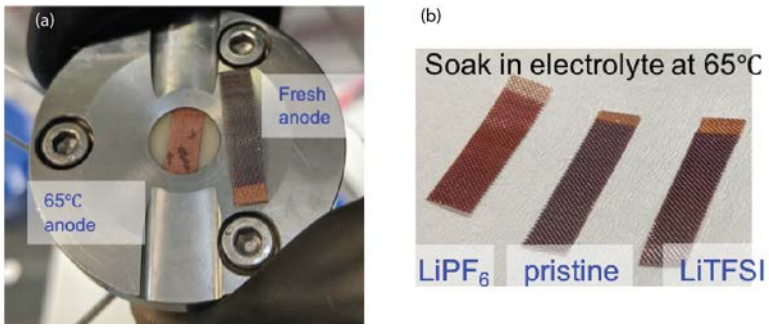

Figure 3. (a) Photograph showing the degraded Si on Cu mesh inside the spectroelectrochemical cell after heating to 70°C. A pristine anode is also shown for comparison. (b) Photograph comparing Si anodes after soaking in either $LiPF_6$ salt or LiTFSI salt 1.2 M in EC:EMC [3:7 wt:wt] solvent and heated to 65°C for 30mins.

As a simple test of their temperature-dependent reactivity, we soaked our a-Si film on Cu mesh electrode in Gen2 electrolyte in a sealed Nalgene bottle while slowly heating on a hotplate to 65°C. The electrode sample was removed after 30 mins at 65°C. We performed the same experiment with 1.2 M LiTFSI salt in the same binary solvent. Figure 3b shows a photograph of the two electrodes, and a pristine sample for comparison. Clearly, the sample heated in Gen2 looks distinctly different from the other two and has undergone some decomposition/dissolution.

Unlike in $LiPF_6$-based electrolyte (Fig. 3b), the SERS spectra of an a-Si/Li half-cell at OCV in LiTFSI-based electrolyte remained unchanged from 25 to 75°C (not shown). Therefore, we performed in-situ SERS at 75°C during galvanostatic cycling with a 15µA applied current (~0.5C rate) between 1.5 and 0.01V (vs. Li/Li^+). Figure 4a shows the voltage profiles for the first two cycles. The colored dots correspond to specific SERS spectra shown in Figure 4b. In LiTFSI-based electrolyte, the measured SERS spectra were unaffected by temperature. Detection of (delithiated) a-Si, the peak at 470cm^{-1}, and observation of SEI species including formation of alkyl carboxylate (e.g. peak at 1565cm^{-1}) was similar to our recently published results using Gen2 ($LiPF_6$) at room temperature.[3] For a-Si thin film anodes, 1.2M LiTFSI in EC:EMC is likely a suitable electrolyte for thermal abuse studies.

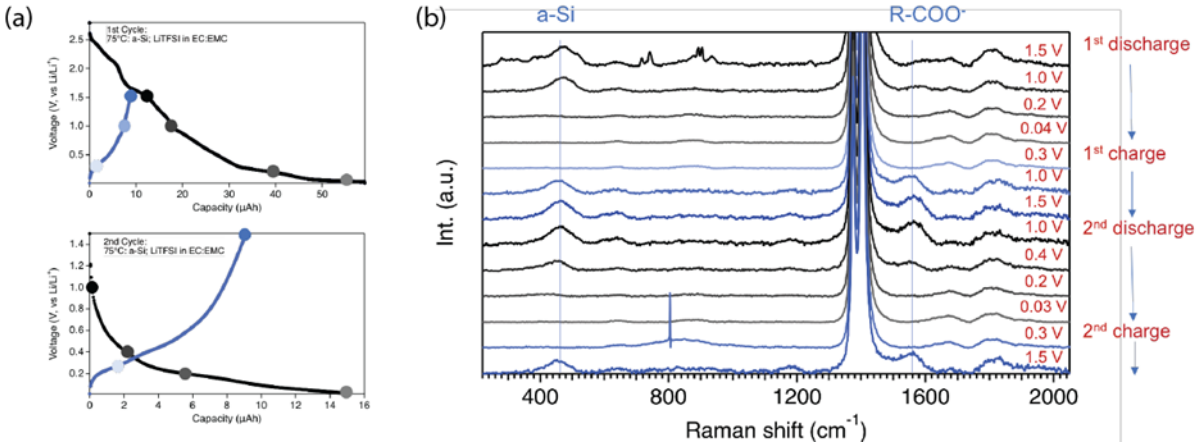

Figure 4. (a) Voltage vs. capacity profiles at 75°C of an a-Si half cell in LiTFSI-based electrolyte. (b) Temperature dependent SERS spectra during the first two electrochemical lithiation/delithiation cycles at 75°C. The colored dots in (a) correspond to specific SERS spectra shown (b).

To ensure the HF reacting and destroying Si is not a thin film specific problem, we tested Si composite electrodes (CAMP, A-A018, Si(80):C45(10):LiPAA(10)) at 25°C and 70°C in 2032-type coin cells. The Si/Li half-cells were cycled in $LiPF_6$- or LiTFSI-based electrolytes. After a 2 hours OCV rest, the cells were subjected to

galvanostatic cycling at C/20 between 1.5 and 0.01V (vs. Li/Li^+) for 3 cycles. Afterwards, the cells were disassembled and the recovered anodes were soaked in DMC for 60 seconds to remove residual electrolyte, then the surface of the anodes was analyzed with scanning electron microscopy (SEM), energy dispersive spectroscopy (EDS) and x-ray photoelectron spectroscopy (XPS).

The voltage profiles (Figure 5a) show all cells were successfully discharged and charged for 3 cycles, higher capacity was attained at 70°C in both $LiPF_6$- and LiTFSI-based electrolytes, and that LiTFSI at 70°C exhibited the highest capacity retention during the first 3 cycles. After cell disassembly, the electrodes were photographed, as shown in Figure 5b. In the case of Gen2 at 70°C, the lithium metal showed severe discoloration, possibly due to side reactions from PF_6 decomposition. Li metal color change was much less in LiTFSI-based electrolyte at 70°C, but a thick opaque layer (SEI) formed on the Si electrode surface. These results suggest large electrolyte decomposition at 70°C in both $LiPF_6$- and LiTFSI-based electrolytes.

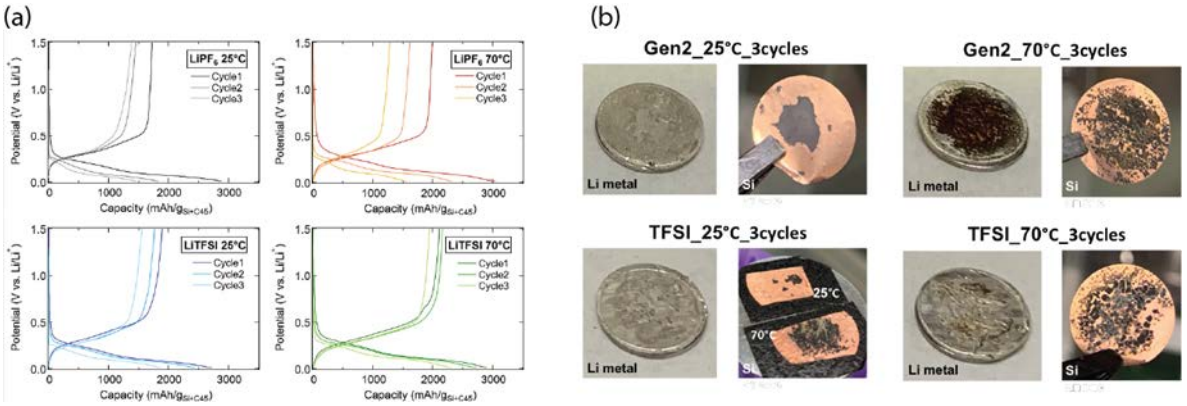

Figure 5. (a) Voltage vs. capacity profiles for Si/Li half-cells were cycled in $LiPF_6$- or LiTFSI-based electrolytes at 25°C and 70°C. (b) Photographs of the electrodes after cycling.

SEM images of the anodes are shown in Figure 6a. The images confirm that the surface layers formed during the first 3 cycles are more prevalent at higher temperature. EDS measurements of the electrodes (Figure 6b) reveal higher concentrations of fluorine and phosphorous particularly in the case of Gen2 at 70°C (vs 25°C). For LiTFSI-based electrolyte, EDS detects elevated concentrations of sulfur and oxygen at 70°C. XPS also confirms thicker SEIs are formed and extensive electrolyte decomposition occurs at 70°C compared to 25°C.

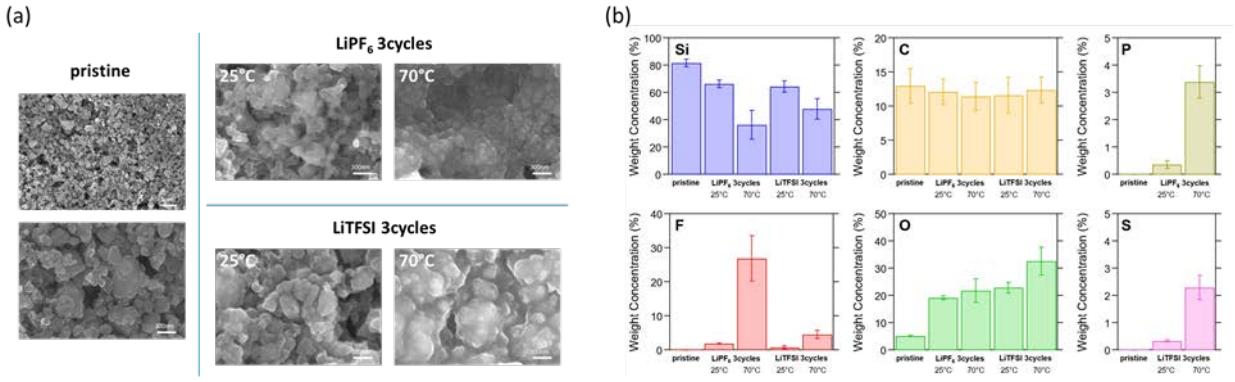

Figure 6. (a) SEM images of Si composite electrode surface after three cycles in LiPF¬6- or LiTFSI-based electrolytes at 25°C and 70°C. (b) EDS analysis of surface composition.

Future electrolyte work includes:

1. Testing GenF (Gen2 + 10 wt% FEC) in addition to Gen2, as a recent paper from Ira Bloom's group showed that the presence of FEC makes the cells less temperature-sensitive. (Piernas-Munoz et al. "Effect of temperature on silicon-based anodes for lithium-ion batteries" J. Power Sources 441 (2019) 227080) VC is another candidate – DSC studies showed that both VC and FEC create a compact SEI layer which enhances the thermal stability. (Profatilova et al. "Enhanced thermal stability of a lithiated nano-silicon electrode by fluoroethylene carbonate and vinylene carbonate" J. Power Sources 333 (2013) 140-149)
2. Test additives such as LiBOB and its derivatives (e.g. LiDFOB) which exhibit better thermal stability than LiPF6 in organic solvents. Also, there's a paper where the Si full-cell capacity retention was enhanced in the presence of 1 % LiFOB in LiPF6-based electrolyte at 45°C and the storage performance was enhanced at 60°C. (Lee et al. "A bi-functional lithium difluoro(oxalate)borate additive for lithium cobalt oxide/lithium nickel manganese cobalt oxide cathodes and silicon/graphite anodes in lithium-ion batteries at elevated temperatures" Electrochim. Acta 137 (2014) 1-8)
3. If we were to confirm if Si is disappearing due to the formation of HF, then we could test LiBF4 which is also moisture-sensitive – more of a follow-up study on HF formation than improving the Si safety.

Conclusions

We would like to understand the factors that affect safety in silicon anode LiBs, with a specific focus on highly exothermic reactions that occur at the silicon electrodes. Following up from our initial observations of the instability of a-Si thin films in heated Gen2 electrolyte, we used *in-situ* surface-enhanced Raman microscopy to track the disappearance of the a-Si scattering peak at around 68°C in Gen2 electrolyte. We investigated LiTFSI salt as a potentially more stable electrolyte to enable high-temperature studies of Si anodes. In LiTFSI-based electrolyte, the measured in-situ SERS spectra were unaffected by temperature, even when lithiation/delithiation cycling at 75°C. Using other complementary measurements—FTIR, GC-MS, and XPS—we hope to form a mechanistic understanding of the Si decomposition reactions that occur in Gen2 vs LiTFSI-based electrolytes. In addition to the a-Si thin film anodes, we also evaluated Si nanoparticle composite electrode foils. These electrodes survived Gen2 at 70°C and showed electrochemical performance in coin cells, while the a-Si thin film electrodes were destroyed after about an hour. Thus, the composite electrode study shows factors affecting the Si performance may be different when a composite electrode is used instead of a thin film electrode. Because the composite electrode study showed different results from the thin film electrode, we are moving towards using the composite electrode for *in-situ* SERS. One obstacle is the coating has to be thin (30 nm or less) to have the SERS effect. We are planning on varying different parameters, such as the concentration of the active material in the slurry and coating method to fabricate the composite electrode suitable for the SERS measurement. We are also continuing to refine our in-situ Raman cell design to better match the standard coin cell configuration. In addition, we cannot ignore the possibility that the instability of Li metal at a higher temperature may be contributing to the Si performance in half-cells. To understand the true performance of Si at different temperatures, we are testing three different types of cell configurations: (1) Si/Li half-cells; (2) Si/NMC532 full-cells; and (3) Si/Li_xSi symmetric cells. Ultimately, we are developing protocols for electrochemical cycling tests and analytical characterization as a function of elevated temperature for various Si anode LiBs.

References

1. Ha, Y.; Tremolet de Villers, B. J.; Li, Z.; Xu, Y.; Stradins, P.; Zakutayev, A.; Burrell, A.; Han, S.-D., Probing the Evolution of Surface Chemistry at the Silicon–Electrolyte Interphase via In Situ Surface-Enhanced Raman Spectroscopy. The Journal of Physical Chemistry Letters 2020, 11 (1), 286-291.

2. Akgul, F. A.; Akgul, G.; Yildirim, N.; Unalan, H. E.; Turan, R., Influence of thermal annealing on microstructural, morphological, optical properties and surface electronic structure of copper oxide thin films. Materials Chemistry and Physics 2014, 147 (3), 987-995.

Part 2: Understanding Zintl phase stabilization of the SEI

Model Electrodes of Li-Mg-Si Zintl Compounds for Comparison of Silicon-Electrolyte Interphase Chemistry to Silicon (NREL) (Q1 milestone)

Yeyoung Ha, Zhifei Li, Mike Carroll, Glenn Teeter, Jessica Dudoff, Caleb Stetson, Andrew Norman, Fernando Urias, Greg Pach, Chun-Sheng Jiang, Andriy Zakutayev, Nathan Neale, Mowafak Al-Jassim, Sang-Don Han (NREL)

Background

Recently, B. Han and B. Key *et al.* reported an enhanced electrochemical performance of Si powder-based electrodes (with 10 wt % hard carbon additive (C45) and 10 wt % lithium polyacrylate binder (LiPAA)) in the presence of 0.1 M $Mg(TFSI)_2$ in GenF electrolyte (1.2 M $LiPF_6$ in EC:EMC (3:7 wt%) + 10 wt% FEC).[1] The main idea of this study is the co-insertion of Mg and Li cations into the Si electrode during the lithiation process, forming less-reactive metal-substituted lithium silicide species in an *in situ* manner and reducing the reactivity of charged Si anodes, which result in improved electrochemical performance. Post-electrochemistry characterizations demonstrate that adding Mg secondary salt leads to the co-insertion of Mg cation along with Li into Si during the lithiation process to form relatively stable Li-Mg-Si ternaries. Further *ex situ* (and *in situ*) characterization, however, are still required to address these questions for a better understanding of Li-Mg-Si Zintl phase within a silicon-electrolyte interphase (SiEI):

- What is the formation mechanism of Li-Mg-Si Zintl phase?
- What is the effect of Li-Mg-Si Zintl phase on SiEI?
- What is the role of MgO in SiEI?

Due to the complexity of the SiEI and decomposition products as well as active materials, binder, and conductive carbon in composite electrodes and the limited characterization capabilities with composite electrodes, there is a need for study of model electrodes such as a silicon wafer, an amorphous silicon thin film, and a silicon nanoparticle instead of Si composite electrodes. In addition, the cation and anion of the secondary salt, the starting Si material, the electrolyte solvent choices can have effects on the electrochemical performance of silicon full cell, so more systematic and fundamental studies are critically required.

Results

Preparation of Li-Mg-Si Zintl Phase Model Systems Using a Si Wafer.

We performed X-ray photoelectron spectroscopy (XPS) analysis of electrochemically treated Si composite electrodes (1-cycled, 200 mV-lithiated, and 10 mV-lithiated in GenF and GenFM, respectively) in FY19-Q4. While we observed differences in the XPS spectra from samples prepared in GenF and GenFM, it was difficult to draw a clear conclusion as the system was quite complicated, involving multiple components in the electrode (i.e., Si powders, conductive carbon, and binder). Thus, in this quarter we prepared a model system using Si wafer electrodes to deconvolute the complex XPS spectra and obtain a better understanding of the SiEI (in particular, chemical composition) and the Zintl phase formation mechanism in the presence of $Mg(TFSI)_2$.
Si wafer electrodes (6 mm × 6 mm × 675 μm, 0.001-0.005 Ω cm, p-type (B), 1.3 nm native oxide layer on the surface) and Li metal foil electrodes were used to assemble the Si/Li half-cells (2032 coin-type cells). Two different electrolytes, GenF and GenFM (GenF + 0.1 M $Mg(TFSI)_2$) were tested. After 2 hours of rest at the

open circuit voltage (OCV), the cells were galvanostatically discharged at 100 μA/cm^2 for 2 hours. Then, potentiostatic hold at 10 mV was performed for 40 hours. The electrochemical behavior of the Si/Li half-cells in GenF and GenFM are presented in Figure 1. During the potentiostatic hold, GenFM showed an initial spike in the current followed by a gradual decay while GenF exhibited continuous growth of the current. The lithiated cells were disassembled and the Si wafer electrodes were soaked in 1 mL dimethyl carbonate (DMC) for 60 s to remove residual electrolyte on the surface. The samples were transferred to the XPS instrument without exposure to air.

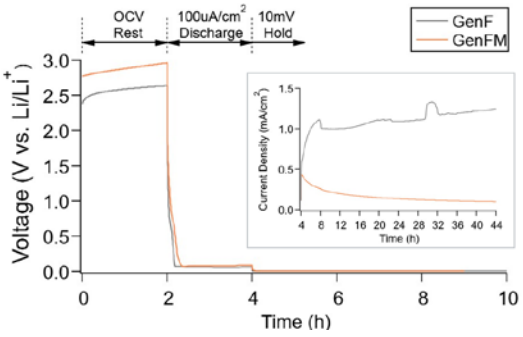

Figure 2. Electrochemical behavior of Si wafer electrodes in GenF (gray) and GenFM (orange) electrolytes during OCV rest (2 h) → 100 μA/cm^2 galvanostatic discharge (2 h) → 10 mV potentiostatic hold (40 h).

Previous XPS analysis (FY19-Q4) of the cycled Si composite electrodes demonstrated the presence of Li_xSi at the surface of GenF samples while it was absent at the surface of GenFM samples. It is noted that, however, Raman can detect 385 cm^{-1} peaks attributed to lithium silicide (Li_xSi) in both 10 mV-lithiated GenF and GenFM samples. In 10 mV-lithiated GenFM samples, we observed a Mg 2p peak at ~50.5 eV which may be assigned to the Li-Mg-Si Zintl phase or a metallic Mg. Considering similar XPS sensitivity factors of Mg and Si (0.252 and 0.283, respectively) the Mg 2p peak is less likely to be from the Li-Mg-Si Zintl phase because we did not observe any peak from the Si 2p core level in the same sample. Instead, it is likely originated from the metallic Mg from possible Mg electroplating during the extensive voltage hold at 10 mV (Li/Li$^+$, hereafter), which is more negative than the standard reduction potential of Mg^{2+} (67 mV *vs.* Li/Li$^+$). In addition to the cycled Si composite electrodes, the cycled Si wafer electrodes also show similar XPS analysis data. One possible explanation for this is that a surface sensitive XPS technique cannot detect the possibly formed Li-Mg-Si Zintl phase in the presence of a top passivation layer mainly composed of MgO (and $MgCO_3$). Thus, we performed XPS depth profiling on the lithiated Si wafer samples to access the 'near' surface of Si electrode. Ar^+ ion sputter was used to remove the formed SiEI layer (including the top passivation layer) with the XPS spectra collection in every 2 nm depth. The XPS depth profile data of GenF and GenFM samples are shown in Figures 2 and 3, respectively. One major difference between GenF and GenFM depth profiles is that the dramatic XPS peak

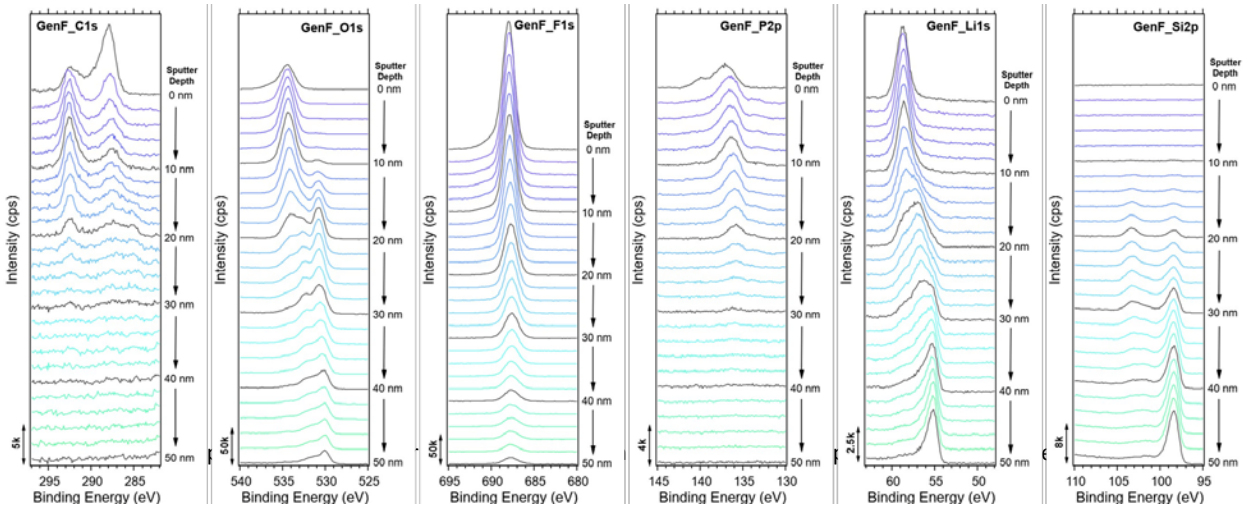

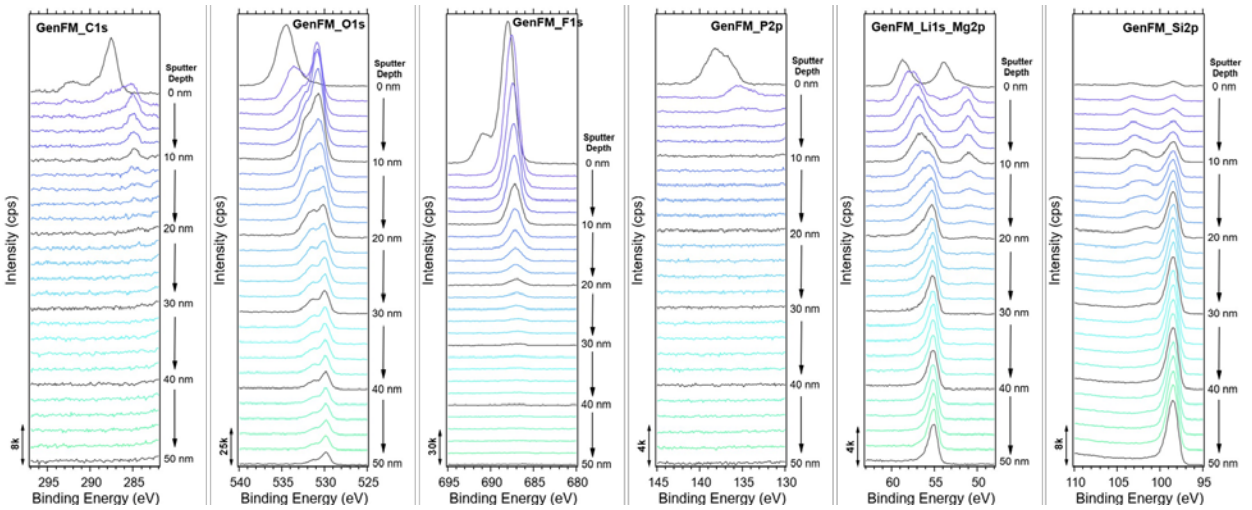

Figure 3. XPS depth profile of Si wafer electrode lithiated in a GenFM electrolyte (spectra collected in every 2 nm depth).

changes are observed between 10 and 30 nm in the GenF sample, while the considerable changes are observed between 0 and 10 nm in the GenFM sample. Moreover, weak Si 2p core level peaks are visible from the beginning in the GenFM sample while the peaks start to appear around 10 nm in the GenF sample. These observations indicate that a relatively thinner and stable passivation layer, likely composed of MgO (and $MgCO_3$), is formed in the GenFM electrolyte, which can be correlated to the observation of 'weak' Si 2p core level peaks and the smaller and gradually decaying current observed during the potentiostatic hold (no further electrolyte decomposition after passivation layer formation).

Detailed analysis of the XPS spectra of GenF and GenFM samples at selected depths are presented in Figures 4 and 5, respectively. For the GenF sample, spectra collected at 0, 10, 20, 30, 40, and 50 nm depth are analyzed. For the GenFM sample, as the peaks shift significantly even after one sputter cycle, spectra collected at 0, 2, 4, 6, 10, 20, and 30 nm are selected for the analysis. In the GenF sample, strong peaks from the SiEI layer (organic species in the C 1s core level, LiF in the Li 1s and the F 1s core levels, and (fluoro)phosphates in the P 2p core level) are observed at 0 nm (without any sputtering). All peaks show ~3 eV charging. At 10 nm sputtered depth, carbonate peaks (C 1s and O 1s peaks at ~292.5 eV and ~534.5 eV, respectively) becomes more intense while the other SiEI component peak intensities decrease. The signals of SiEI components above mentioned are decreased significantly between 20 and 30 nm depth, and the Si 2p core level peaks start to appear in this region. Both lithiated and non-lithiated Si and SiO_x species are present in 20-30 nm depth, and SiO_x is no longer detected in 40-50 nm depth. The Li_xSi peak (~95.2 eV) continuously increase from 20 to 50 nm sputter depth, and the corresponding peak in the Li 1s core level (~55 eV) follows the same trend. Another noticeable feature in depth profiles is that the initial ~3 eV charging observed in all peaks were changed differently upon different species. For example, at 10 nm depth there is no longer charging in the P 2p core level peaks and at 20 nm depth C-C/C-H, C-O, and O=C-O peaks do not exhibit any charging. On the other hand, CO_3 and LiF peaks continue to exhibit the ~3 eV charging throughout the entire sputter depth.

In the case of GenFM sample, similar trends/features upon sputtering—decrease of the peak intensities from SiEI species, increase in the (lithiated) Si and SiO_x species signals, and changes in the initial ~3 eV charging—are observed as shown in the GenF sample, at a much earlier stage of sputtering (0-10 nm depth). For example, the shifts in the C-C, C-H, C-O, O=C-O peaks in the C 1s core level are observed after one sputter cycle (at around 2 nm depth), and the peaks from SiEI components (e.g., organic species, LiF, and (fluoro)phosphates) show significant decrease within 10 nm range. Another major difference between the GenF and GenFM samples are the existence of Mg 2p core level peaks. Initially, two peaks at ~54 eV and ~52 eV, assigned to MgO and metallic Mg (Mg^0), respectively, are present. Upon sputtering, however, the lower binding energy peak (~50 eV, Mg^0) disappears and the higher binding energy peak (~54 eV, MgO) shifts to ~51.5 eV based on overall peak shift. The MgO peak (~51.5 eV) intensity continuously decreases until 10 nm depth and almost disappears at 20 nm depth. Those behaviors (i.e., peak shift to a lower binding energy at 2 nm depth and intensity changes

upon sputtering) can also be observed for other SiEI components, so we can conclude that MgO exists in the SiEI. It is tempting to assign the initial Mg^0 peak (~52 eV) to the Zintl phase, but Mg^0 peak disappears at 2 nm depth while other SiEI component peaks still exist until 10 nm as shown in the C 1s, O 1s, F 1s, P 2p, Li 1s core levels. Thus, it is more likely that this peak results from Mg plating during the potentiostatic hold at 10 mV, as described above.

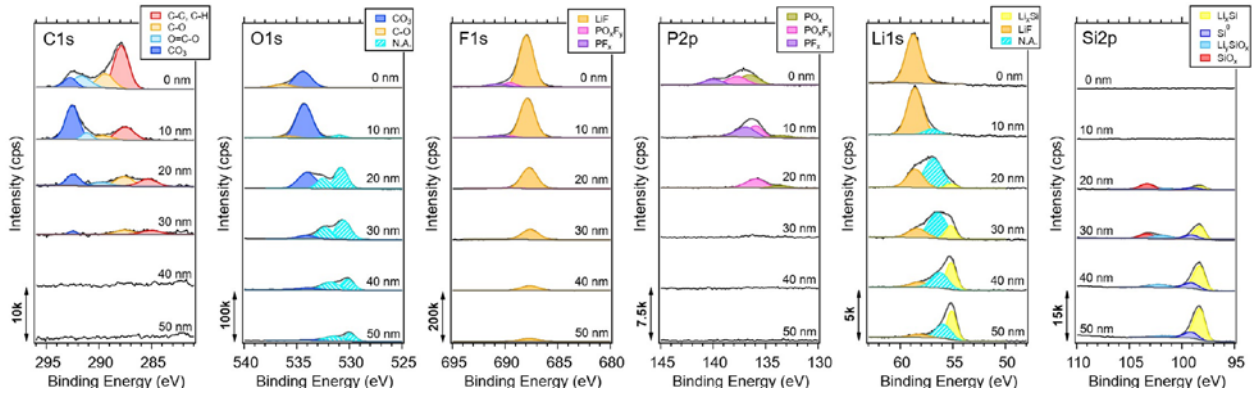

Figure 5. Selected XPS spectra of Si wafer electrode electrochemically lithiated in a GenF electrolyte. Spectra collected at 0, 10, 20, 30, 40, and 50 nm depth are presented (from top to bottom). Black line is the raw spectrum and the gray line is the fit. Peak assignments are preliminary.

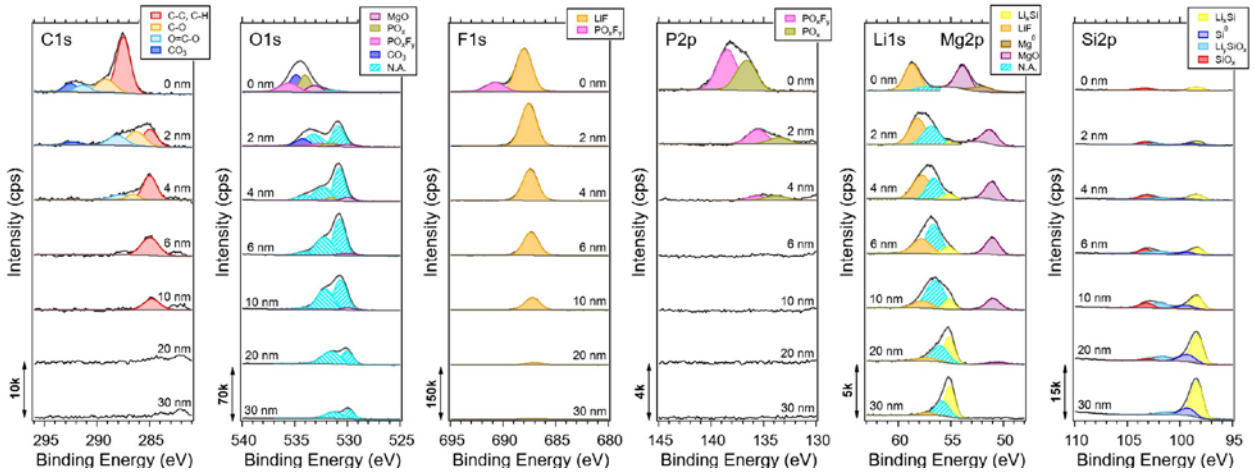

Figure 4. Selected XPS spectra of Si wafer electrode electrochemically lithiated in a GenFM electrolyte. Spectra collected at 0, 2, 4, 6, 10, 20, and 30 nm depth are presented (from top to bottom). Black line is the raw spectrum and the gray line is the fit. Peak assignments are preliminary.

Finally, we examined the effect of dimethyl carbonate (DMC) rinsing step for the electrochemical treated electrodes on the surface chemistry of the electrodes using XPS analysis. The Si wafer electrodes were lithiated in the GenFM electrolyte following the electrochemical protocol (as shown in Figure 1) with two different 10 mV hold time (0 and 10 h). The XPS spectra of four samples with and without DMC rinsing step—soaking the electrodes for 60 s—are presented in Figure 6. In the case of non-rinsed samples (noted as "w/o DMC"), the intense peaks (e.g., CF_3 and TFSI) originated from $Mg(TFSI)_2$ salt are observed in C 1s (~295.5 eV), N 1s (~402 eV), S 2p (~172 eV), and F 1s (~691 eV). Moreover, the intensity of Si 2p core level signal is relatively weaker in the non-rinsed samples and the additional peaks (not assigned) appear in the F 1s (~689 eV) and P 2p (~140 eV), indicating that the residues (mostly $Mg(TFSI)_2$ salt and possibly decomposed electrolyte species) on the electrode surface may block the XPS signals from a SiEI layer. Based on the results, we think the 'gentle' DMC

rinsing step is required for detailed *ex situ* analysis of electrochemical treated electrodes, and we believe *in situ* analysis capabilities should be developed in order to truly understand the chemistry, nature, and properties of the SiEI with respect to its natural occurrence in the battery system.[2]

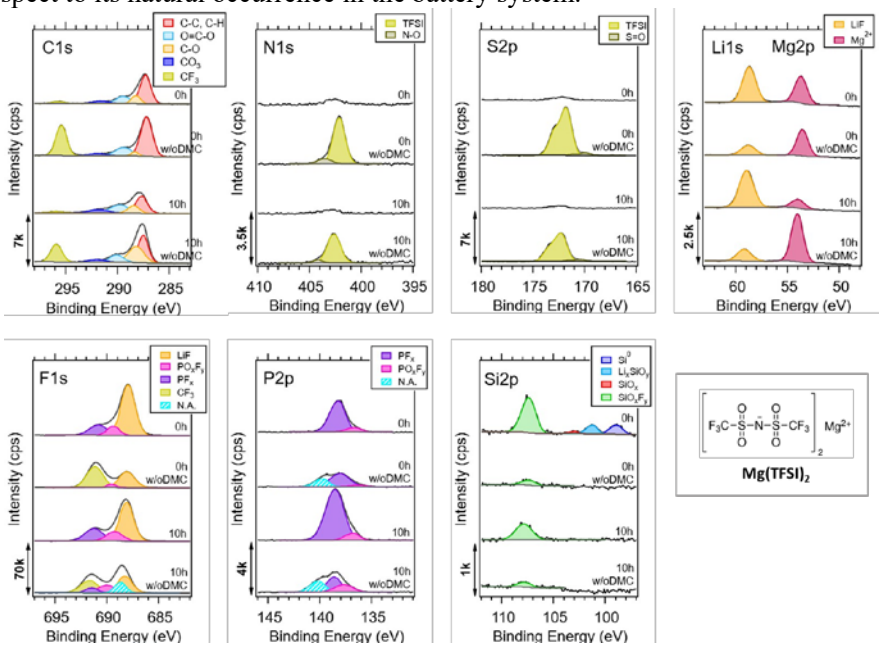

Figure 6. XPS spectra of electrochemical lithiated Si wafer electrodes with and without the DMC rinsing step. Black line is the raw spectrum and the gray line is the fit. Peak assignments are preliminary.

Amorphous Silicon Thin Film with Mg Coating as Model Electrode for Mg-Si Zintl Phase.

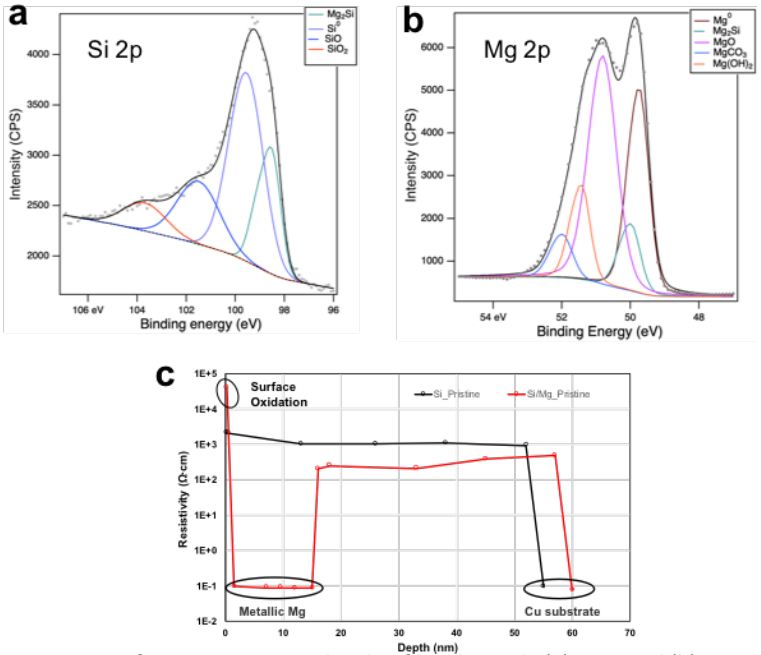

Figure 7. High resolution XPS spectra of pristine Mg coated Si thin film electrode (a) Si 2p and (b) Mg 2p. (c) SSRM resistivity *vs.* depth profile of pristine Si and Mg coated Si thin electrodes.

To prepare the Mg coated Si thin film, RF magnetron sputtering was used to first prepare 50 nm Si thin film on copper substrate and then coat 20 nm Mg on top of the Si thin film. Both the Si and Mg deposition was performed under room temperature with a base pressure of ~2×10^{-7} torr and working pressure of 5 mtorr Ar. The Si and Mg were deposited with a working distance of 8 and 10 cm, and sputtering power of 4.5 and 1.3 W/cm^2, respectively. The deposition chamber is coupled with glovebox and therefore, the Si film did not expose to air before Mg deposition.

The Mg coated Si anode was first characterized by XPS and scanning spreading resistance microscopy (SSRM). Mg_2Si was observed from both the Si 2p and Mg 2p spectrum (Figures 7a and b). Mg_2Si typically cannot be formed under room temperature. However, as the Mg was deposited onto Si under Ar atmosphere and the Si surface did not expose to air before Mg deposition, it is possible to form a thin layer of Mg_2Si under such condition.[3, 4] The SSRM resistivity *vs.* depth profile reveals a sharp contrast of the Si electrode before and after Mg coating. As shown in Figure 7c, the Mg coated Si electrode has a higher resistivity on the top surface which should be attributed to thin surface MgO_x layer as a result of the Mg oxidation. The resistivity of Mg coated Si electrode drops to a much lower value after this surface oxidation layer as metallic Mg has much lower resistivity than Si. Interestingly, even though the resistivity of the Mg coated Si electrode increased after the Mg layer, it is still lower than pure Si anode through the bulk Si layer. This result suggests that Mg had diffused into the bulk Si layer reducing its resistivity. Although there is no direct correlation between Mg diffusion into Si layer and the formation of Mg_2Si, the fact that Mg can diffuse into the bulk Si layer would at least support the possible formation of Mg_2Si.

To further confirm the diffusion of Mg into the bulk Si layer, we collected the scanning transmission electron microscope (STEM) high-angle annular dark-field (HAADF) image and energy dispersive spectroscopy (EDS) atomic maps of the cross-section of the Mg coated Si thin electrode (Figure 8). The EDS atomic maps of different elements were performed on the same region as in the HAADF image. The Cu substrate and the top Pt layer which was deposited before performing focus ion beam (FIB) is clearly shown, and the Si and Mg layers are in between the Cu and Pt layers. As shown in Figure 8, the Mg layer is thinner than the Si layer, where part of the Mg layer is on top of the Si layer, and part of it overlaps with the top to middle part of the Si layer, indicating the existence of a pure Mg layer and the possible diffusion of Mg into the bulk Si layer. Note that from the atomic mapping of Si and Mg, it seems like that there is no Mg. However, this may not necessarily mean that there is no Mg at all in this region, and it could be just the Mg concentration is low in this region. The elements mapping result agrees well with the dramatically decrease of the resistivity after the initial surface oxide layer and the slightly increase of the resistivity of the Mg coated Si from the middle to the bottom of the Si layer (Figure 7c). The oxygen mapping suggests that the Pt deposition process had introduced a relative high oxygen level, and it also reveals a relative high oxygen content at the Si/Mg and Si/Cu interfaces, which should be due to the surface oxides. Overall, the XPS, SSRM and EDS mapping results suggest that the coated Mg on Si would form thin layer Mg_2Si with Si and the coated Mg is able to diffuse into the bulk Si layer.

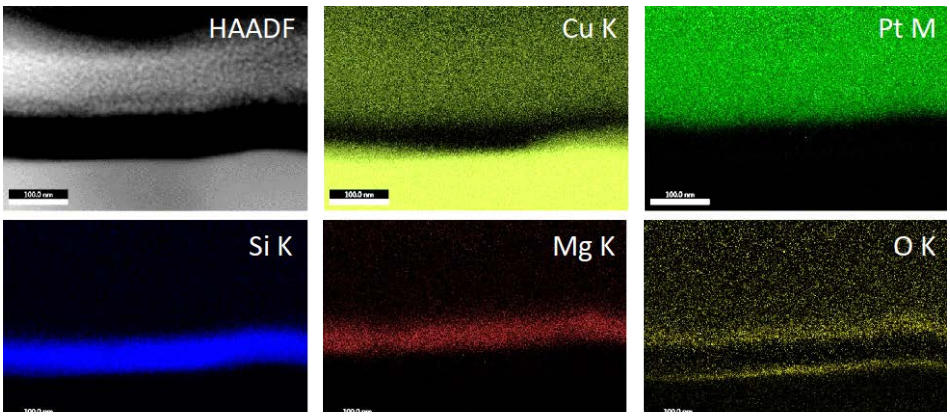

Figure 8. SETM HAADF image and EDS atomic maps of pristine Mg coated Si electrode.

The obtained Mg coated Si thin film was electrochemically cycled in a Li half-cell with Gen2 (1.2 M $LiPF_6$ in EC:EMC, 3:7 wt%) and GenF electrolytes, and Si thin film without Mg coating was also cycled in Gen2, GenF and GenFM (GenF with 0.1 M $Mg(TFSI)_2$) electrolytes for comparison. The first reversible capacities of both Si and Mg coated Si electrodes in Gen2 electrolyte are lower than those in GenF or GenFM electrolyte (Figure 9a). This may be caused by higher polarization of the electrodes possibly due to the formation of a less ion conductive SiEI layer with Gen2 electrolyte, which needs further investigation. The shape of the charge-discharge profiles is similar for Si and Mg coated Si thin film electrodes in different electrolytes, where the Mg coated Si shows a small plateau at low potential during delithiation in Gen2 electrolyte. This may be due to the dealloying process of Li-Mg and it is still not clear why it only shows in Gen2 electrolyte. The C-V curves (Figure 9b) reveal that Mg coated Si has the largest polarization, where during the first cathodic scan the two Li-Si alloying peaks merged into one. This indicates that the coated Mg layer, especially the oxidized top layer, may act as a barrier for Li-ion diffusion. The Si anode in GenFM electrolyte also exhibits a higher polarization, which suggests that adding $Mg(TFSI)_2$ salt in the GenF electrolyte may induce a more ion resistive SiEI layer.

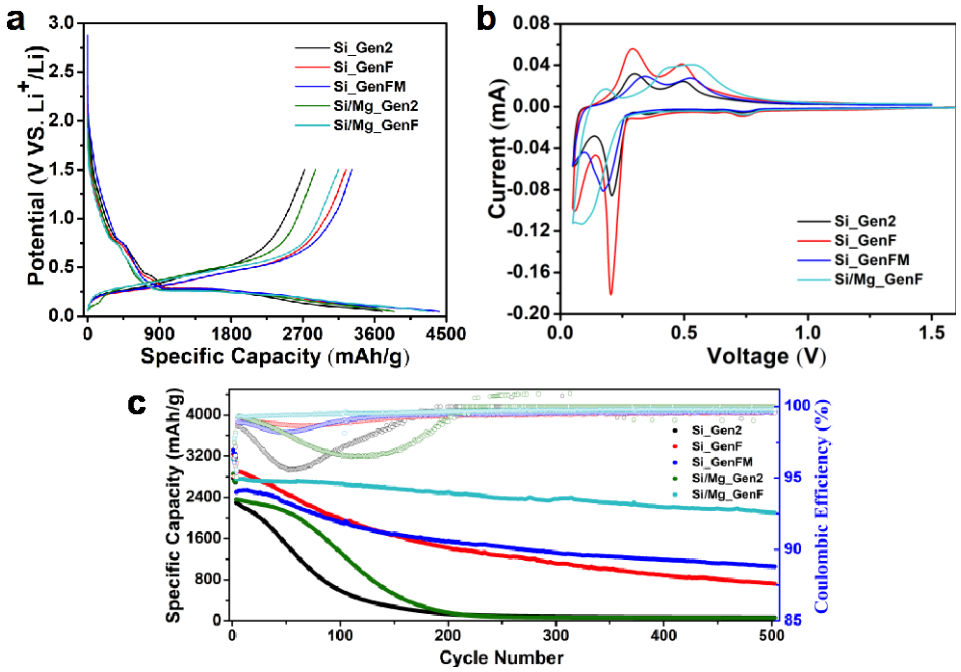

Figure 9. Electrochemical performance of Si and Mg coated Si electrodes in the potential range of 0.05-1.5 V in different electrolytes: (a) First cycle galvanostatic charge-discharge profiles at the current density of 0.1 C (3.9 μA/cm²), (b) cyclic voltammetry curves at scan rate of 0.1 mV/s, (c) cycling performance with 3 formation cycles at 0.1 C and then aging cycles at 1 C.

The electrochemical cycling tests of Si and Mg coated Si thin film electrodes were performed at 0.1 C for 3 formation cycles and then at 1 C for 500 aging cycles. As shown in Figure 9c, even though Mg coating improved the cycling performance of Si anode, it still faded quickly in Gen2 electrolyte, which is much worse than the cycling performance in GenF electrolyte. As the coulombic efficiency of both Si and Mg coated Si electrodes in Gen 2 electrolyte is much lower than those in GenF electrolyte, the failure of the cell with Gen2 should be caused by the quick consumption of electrolyte, indicating that adding FEC is necessary to form a more effective and robust SiEI on Si electrodes. The capacity retention of Si electrode was improved from 25% to 42% by adding $Mg(TFSI)_2$ salt in GenF electrolyte, however, the reversible capacity of Si electrode was lower in GenFM electrolyte. In contrast, the Mg coated Si electrode in GenF electrolyte remained 76% of the capacity after 500 cycles which is much higher than the Si electrode without Mg coating or the Si electrode in GenFM electrolyte. The fact that Mg coated Si electrode can reach a higher and stable coulombic efficiency after the initial cycles, suggesting that Mg coating can improve the stability of the SiEI layer and the subsequent cycling stability.

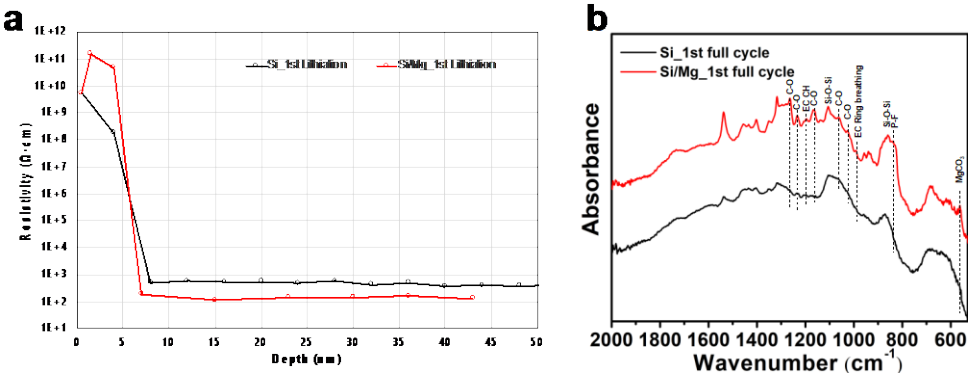

Figure 10. (a) SSRM resistivity *vs.* depth profile of Si and Mg coated Si electrodes after the first lithiation at 0.1 C in a GenF electrolyte. (b) FTIR spectra of Si and Mg coated Si electrodes after the first full cycle at 0.1 C in a GenF electrolyte.

For mechanistic understanding of improved cycling stability of Mg coated Si electrode, SSRM resistivity *vs.* depth profile and FTIR spectra were collected after cycling. As shown in Figure 10a, after the first lithiation, the resistivity of the surface layer increased a lot for both Si and Mg coated Si electrodes, which should be due to the formation of SiEI layers. The resistivity drops dramatically after about 8 nm, indicating that the thickness of formed SiEI layer is around 8 nm. Note that the SiEI resistivity of the Si electrode with Mg coating is higher than that of the uncoated one, suggesting that Mg coating may lead to the SiEI layer with different components. The FTIR spectra of the Si and Mg coated Si electrode after the first full cycle demonstrate the difference of their surface species (Figure 10b). The Mg coated Si electrode shows additional peaks compared with uncoated one, and those peaks are mainly attributed to C-O stretching derived from ethylene carbonate (EC) molecules and the decomposition products of EC. Overall, our obtained data suggest that Mg coating has changed the components of the SiEI layer, which may be responsible for the improved cycling performance of the Mg coated Si electrode. Further detailed analysis is undergoing to check what other changes (e.g., chemical composition and properties) Mg coating had introduced into the SiEI layer.

Silicon Nanoparticle Size, Surface, and Electrolyte Effects on the Capacity Retention in Air-Free Si Nanoparticle Electrodes.

Our previous capability development efforts to enable air-free fabrication of silicon-based Li-ion half cells has been exploited to study the effect of surface oxidation on capacity fade rates for non-thermal RF plasma grown silicon nanoparticles (Si NPs) of various sizes in different electrolytes. We have previously shown that when we expose Si NPs with a size < 7 nm to water, the entire Si NP converts to SiO_x which has no measurable Li-ion storage capacity. We can therefore now systematically investigate how an interfacial layer of SiO_x affects the SiEI electrochemical properties (since we can rule out any contribution of SiO_x to the reversible cycling). In addition, the success of the Li-Mg-Si Zintl phase reactivity studies on one batch of Paraclete Si NP-based anodes has prompted the question: Will similar SiO_x-terminated surface chemistries between Paraclete and plasma-grown (and intentionally oxidized) Si NPs enable similar improved capacity retention with $Mg(TFSI)_2$ additive? This question is aligned with the Q1 milestone: Have demonstrated ability to make model electrodes of Mg-Si Zintl compounds and compared SiEI chemistry to silicon using XPS, STEM-EDS and FTIR/Raman.
We carried out a series of parametric experiments on varied sizes of Si NP-based composite electrodes (grown by the non-thermal RF plasma method) with and without the presence of a 2–3 nm thick native oxide layer on the surface of the Si NPs (grown by methods described in the FY19-Q3 report). Using the cycling protocol: 3 formation cycles at C/20 and 100 aging cycles at C/5, experiments measuring the capacity fade of these electrodes were carried out in three different electrolytes; Gen2, Gen2 + 10% FEC (GenF), and Gen2 + 10% FEC + 0.1 M $Mg(TFSI)_2$ (GenFM). The normalized (at cycle number = 4) capacity data is shown for all three

electrolytes in Figure 11a. From these data, it is clear that the electrodes containing the smallest Si NPs display the greatest overall capacity retention, regardless of the surface termination (air-free "SiH_x" *vs.* SiO_x) or electrolyte, but the overall capacity retention is greatest for composite electrodes in GenF electrolyte followed by GenFM, and finally Gen2. To quantify the lifetimes of these size- and surface-dependent Si NPs anodes, the data in Figure 11a was fit to an exponential function. The lifetimes from the fits are shown in Figure 11b.

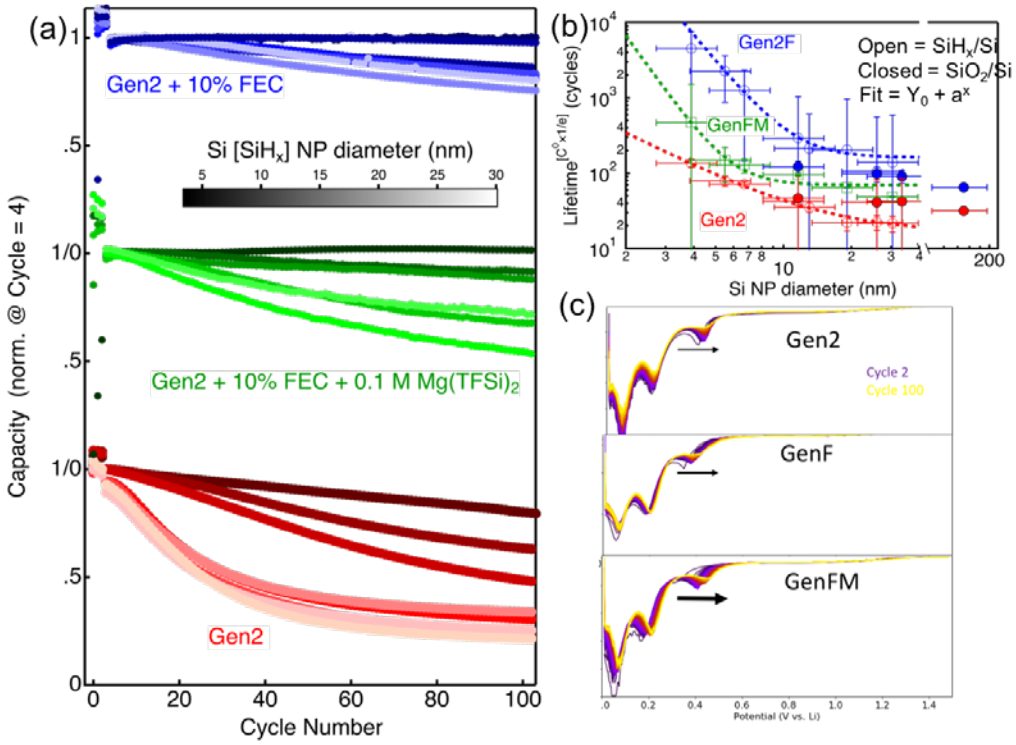

Figure 11. (a) Normalized capacity *vs.* cycle number data for a size range of Si NP-based composite electrode half cells with GenF (blue), GenFM (green), and Gen2 (red) electrolytes. (b) Lifetimes extracted from fitting the capacity fade data in panel (a). The open shapes correspond to Si NP electrodes with air-free "SiH_x" surfaces and the close shapes are those with intentionally oxidized SiO_x surface termination. The vertical error bars are the errors from the fits and the horizontal error bars are $\pm 1\sigma$ from the mean of the average Si NP size. The dashed lines of the same color are power fits to the SiH_x data. (c) Consecutive dQ/dV data for lithiation of 3.9 nm SiHx-terminated silicon electrode half cells in the three electrolytes measured. The arrows are a qualitative indicator of the positive shift of the lithiation features with increasing cycle number. The bigger arrows indicate a large positive shift. The table below Figure 11 is the fitted values from the data in Figure 11b.

Table-1: Values obtained from fitting data in Figure 11b.

	Gen2	GenF	GenFM
a (nm^{-1})	950	1.0×10^6	1.23×10^5
x	-1.5	-3.6	-4.2

The data in Figure 11b show that the measured capacity fade rates depend on both the Si NP size as well as the electrolyte. The cycle lifetime of the electrodes of the smallest 3.9 nm-diameter Si NPs of ~4000 cycles is more than ten times greater than the 30 nm diameter Si NPs. The magnitude of this difference is persistent across all electrolytes. We note, however, that obtaining reliable cycle lifetimes when only 100 cycles were measured is difficult, since this gives rise to large error bars on the smallest Si NP data points in particular. Therefore, future experiments measuring capacity fade will be conducted out to 500 cycles to minimize this error and better predict the actual lifetimes.

The electrolyte itself also plays a large and obvious role where GenF shows the longest cycle lifetimes followed by GenFM and then Gen2. For these plasma-grown Si NPs with air-free SiH_x surfaces, the $Mg(TFSI)_2$ additive in GenFM is deleterious to capacity retention (cf. GenF). Thus, other surface chemistries must be responsible for the observed stabilization by $Mg(TFSI)_2$ added electrolyte with one batch of Paraclete. The effect of Si NP size and electrolyte composition was further quantified by fitting the cycle lifetimes with a power fit. The extracted slopes and power law value are shown in Table 1. We do not currently have a concrete understanding of the meaning of these power law values, and we will work with the computational team (Persson, Colclasure) to understand if these values are meaningful and can be correlated with any physical parameters (e.g., strain).
The role of SiO_x is not as obvious as the roles of electrolyte composition and Si NP size. Electrodes based on SiO_x-terminated Si NPs exhibit a diminished capacity retention in GenF electrolyte compared to those based on air-free SiH_x Si NPs, whereas in Gen2 electrolyte this trend is reversed (SiO_x has better capacity retention than SiH_x). These data indicate that the role of the surface SiO_x on silicon-based Li-ion electrode is complex and also depends largely on the environmental conditions during cycling which likely produces very different SEI layers. Still, it is important to re-emphasize that in all cases GenF is the superior electrolyte.
While the presence of $Mg(TFSI)_2$ in the electrolyte did not improve the overall capacity retention in these electrode half cells with respect to the GenF electrolyte, the signatures of Zintl phase formation were present. One of these signatures can be seen from inspection of the dQ/dV, plotted in Figure 11c. Here we show consecutive lithiation dQ/dV with increasing cycles of identical 3.9 nm-diameter Si NP electrodes in the three electrolytes measured. The peak of the lithiation phases shift positively with increasing cycling indicating a reduced impedance with continued cycling. The magnitude of that shift, however, depends on the electrolyte. The greatest positive shift occurs for the electrolyte with 0.1 M $Mg(TFSI)_2$. This is suggestive of the Mg-Si Zintl phase formation as a smaller kinetic barrier is needed to insert lithium into the amorphous silicon.[1] However, more detailed analysis through FTIR, Raman, and NMR are required to fully characterize the Mg-Si Zintl phase chemistry at these Si NP systems and will be the focus of future work.

Conclusions

XPS depth profile analysis of Si wafer model electrodes lithiated in GenF and GenFM demonstrated the formation of a thinner SiEI layer in GenFM, possibly due to the surface passivation in the presence of $Mg(TFSI)_2$. The source of surface passivation is likely MgO, which was detected as one of the SiEI components. To verify this observation, we have a plan to electrochemically treat the hydrogen-terminated Si wafer electrodes prepared via HF etching of the surface oxides, followed by in-detailed surface and bulk characterization of them. Additionally, we will perform the XPS depth profile analysis on the model Li_2MgSi sample prepared by ANL to refine XPS peak assignment library of the Zintl phase compounds.
The electrochemically treated samples prepared with and without the DMC rinsing step for 60 s were analyzed using XPS, and the non-washed samples showed the intense peaks originated from the residual salt with weaker signals from the Si electrode. Although the DMC washing step may affect the chemistry, nature, and properties of the SiEI, we think it is a required step to remove the residual salt (especially for the surface sensitive XPS measurements), and the current protocol with a rinsing step seems to be effective.
The cycling stability of thin film Si electrode is significantly improved via Mg coating in the GenF electrolyte. Characterization of the pristine Mg coated Si electrode reveals the formation of Mg_2Si and the diffusion of Mg into the bulk Si layer. It is also found that Mg coating may have changed the components of the SiEI layer during the lithiation, which may responsible for the improved cycling stability.
The effect of Si NP size, surface (air-free SiH_x *vs.* intentionally oxidized native SiO_x), and electrolyte were studied through a parametric analysis. We find that the smallest diameter Si NPs display the most robust capacity retention where the effective cycle lifetime exceeds 1000 cycles. Additionally, the best capacity retention is observed when air-free SiH_x Si NP electrodes are paired with GenF electrolyte. The effect of the surface oxide on capacity retention depends on the electrolyte used, with Gen2 electrolyte enabling greater capacity retention for SiO_x- *vs.* SiH_x-terminated Si NPs, but the opposite is true when GenF electrolyte is used (SiH_x better than SiO_x). Future work will firstly conduct similar studies on SiO_x-terminated Si NPs with GenFM electrolyte as well as focus on characterizing the surfaces of these NP electrodes before and after cycling though a combination of FTIR, Raman, and electron microscopies.

References

1. Han, B.; Liao, C.; Dogan, F.; Trask, S. E.; Lapidus, S. H.; Vaughey, J. T.; Key, B., Using Mixed Salt Electrolytes to Stabilize Silicon Anodes for Lithium-Ion Batteries via in Situ Formation of Li-M-Si Ternaries (M = Mg, Zn, Al, Ca). *ACS Appl. Mater. Interfaces* **2019,** *11*, 29780-29790.
2. Ha, Y.; Tremolet de Villers, B. J.; Li, Z.; Xu, Y.; Stradins, P.; Zakutayev, A.; Burrell, A.; Han, S.-D., Probing the Evolution of Surface Chemistry at the Silicon–Electrolyte Interphase via In Situ Surface-Enhanced Raman Spectroscopy. *J. Phys. Chem. Lett.* **2020**, *11*, 286-291.
3. Wigren, C.; Andersen, J. N.; Nyholm, R.; Karlsson, U. O., Epitaxial silicide formation in the Mg/Si(111) system. *Surf. Sci.* **1993**, *289*, 290-296.
4. An, K. S.; Kim, R. J.; Park, C. Y.; Lee, S. B.; Abukawa, T.; Kono, S.; Kinoshita, T.; Kakizaki, A.; Ishii, T., Initial Interface Formation Study of the Mg/Si(lll) System. *J. Appl. Phys.* **1995**, *78*, 1151-1155.

Ex-situ ^{7}Li & ^{29}Si NMR studies on formation and evolution of ternary Zintl phases (Q1 Milestone)

Baris Key, Xiang Li, Fulya Dogan, Steve Trask , James A. Gilbert, Jack Vaughey (ANL)

Background

Silicon is one of the most promising anode candidates for LIBs. However, one of the main problems with Li-Si chemistry in a Li-ion battery is the inherent reactivity of the lithium silicide zintl phases, the active material that forms upon the lithiation. These phases can react with almost all battery components such as binders, electrolytes, additives and impurities such as moisture and air which cause major columbic losses and loss of lithium.The stability of the zintl phases formed can be improved significantly and their reactivity can be controlled by adding 0.1 M MTFSI salts (M =Mg, Al, Zn, Ca) in the electrolyte forming ternary zintl phases in an insitu fashion.. To understand the mechanism of Zintl phases formation upon lithiation/delithiation process, high-resolution ^{7}Li and ^{29}Si NMR is utilized to directly probe the local Li and Si environments.

Results

Extensive effort has been made to study the zintl phase formation and how it affects the thermodynamic stability the silicon anodes.[1-2] Previously, we have successfully demonstrated the effect of substituting different metal cations (Mg, Zn, Al, Ca) into as-prepared lithium silicide and magnesiated lithium silicide.[3] However the formation mechanism and the fundamental chemistry such as, how the dynamic changes upon charge and discharge behind this, is still unknown. Traditional diffraction techniques are more sensitive to heavy atoms and those martials with long range order, which cannot provide enough insights into the Li-related structure and the very amorphous Si after cycling. Here, we use high-resolution solid-state NMR to probe the local Li and Si environments at different state of charge for silicon anodes cycled with Gen2+10%FEC (GF) and Gen2+10%FEC+ 0.1M MgTFSI (GFM) electrolytes. 1st cycle electrochemical performance, high resolution ^{7}Li NMR spectra and the spectral simulation are shown in Figure 1(a), (b), and (c), respectively. Three main lithium environments are observed diamagnetic Li resonating around 0 ppm, due to SEI formation and residual electrolyte, lithiums in isolated Silicon with a peak around 8 ppm and lithium in Silicon clusters observed with a broad peak above 15 ppm. These peaks observed and the assignments correlates well with the previous ^{7}LiNMR studies by Bon Fassler and Clare Grey [4-6] . The peak position and intensity of 8ppm resonance change with the lithiation/delithiation process. Upon the 1st discharge, Li signal at the very early stages is from Li insertion into the surface SiO layer, and it gives a relatively small capacity around 100mAh/g. Li is then inserted into the position close to isolated Si from 0.35V to 0.1V, and as more Li is coordinated with Si, the lithium-7 peak position shifts toward lower field. From 0.1V to the fully lithiated state, Li insertion starts within Si clusters

and possible Li migration from isolated Si to Si clusters accelerates the Li content distribution. Upon 1st charge, Li is first extracted from Si clusters and then isolated Silicons, indicating reversible Li dynamics in Si anode. At the end of 2nd discharge, Li is distributed more uniformly compared to the 1st discharge, especially in the bonded Si clusters. Considering the severe capacity loss for silicon anodes , it is highly possible that isolated Si has less reactivity and reversibility after lithiation/delithiation.

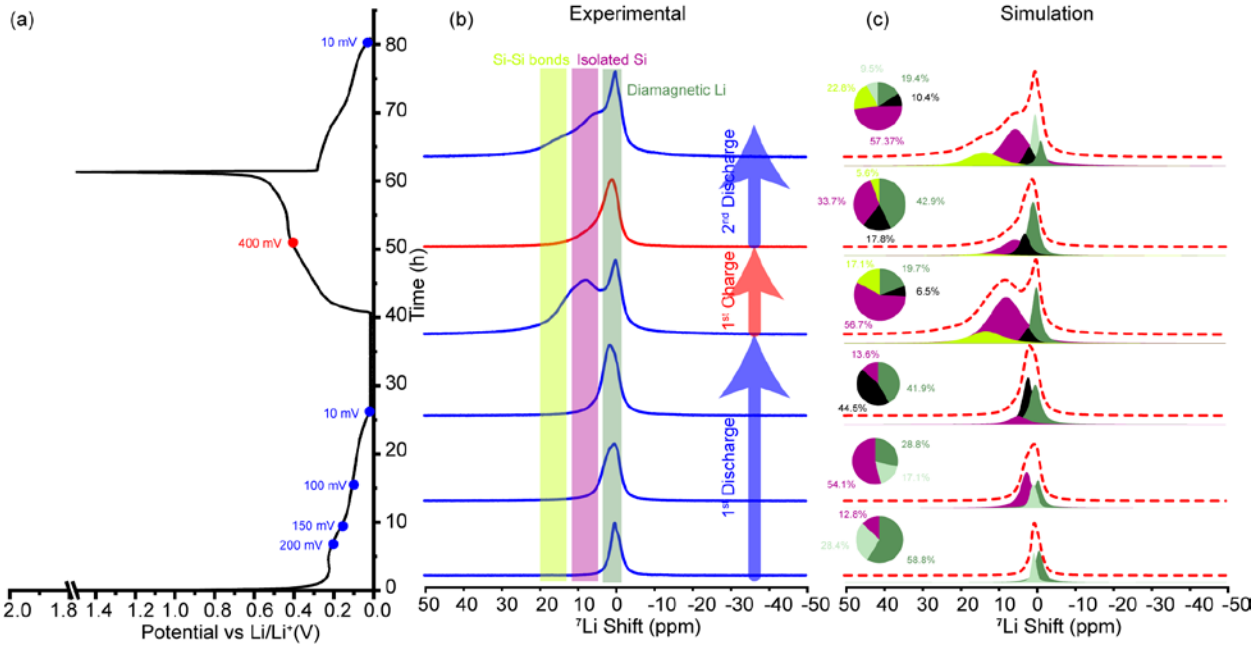

Figure 1. Electrochemistry data (a), *ex-situ* ^{7}Li NMR spectra (b) and the corresponding spectral simulation (c) of GF series.

The addition of Mg^{+2} into the electrolyte facilities the formation of Li-Mg-Si ternary zintl phases during electrochemical cycling which changes the peak positions and intensities observed in 7Li NMR. As shown in Figure 2, ^{7}Li NMR spectra at different charge state in the first 2 cycles were measured with exactly the same condition as GF series. Similarly, upon 1st discharge, Li insertion in SiO layer is first observed at the very beginning, then a broad component resonating around 8 ppm gradually intensify from 0.35V to 0.1V and start to decrease till the end of discharge. On the other hand, Li insertion into Si clusters is observed at 100 mV and continually growing from 9.5% to 32.2%. Additionally, a peak resonating over 30 ppm is seen at the end of discharge which is assigned as Lithiums in over-lithiated Si. Small amount of Zintl phase formation leads to more evenly Li distribution, which may benefit bulk structural reversibility and therefore long-term cycling performance. Upon 1st charge, Li removal starts preferentially from the Si clusters and then isolated Si, which is consistent with our GF series study. In the following discharge, more Li is inserted into Si clusters. Interestingly, the metastable phase at -10 ppm is also observed at the end of 2nd discharge, this over-lithiated $Li_{15+x}Si_4$ is highly reactive and would not be captured until stabilized. This key observation indicates that Zintl phase help establish the thermodynamic stability.

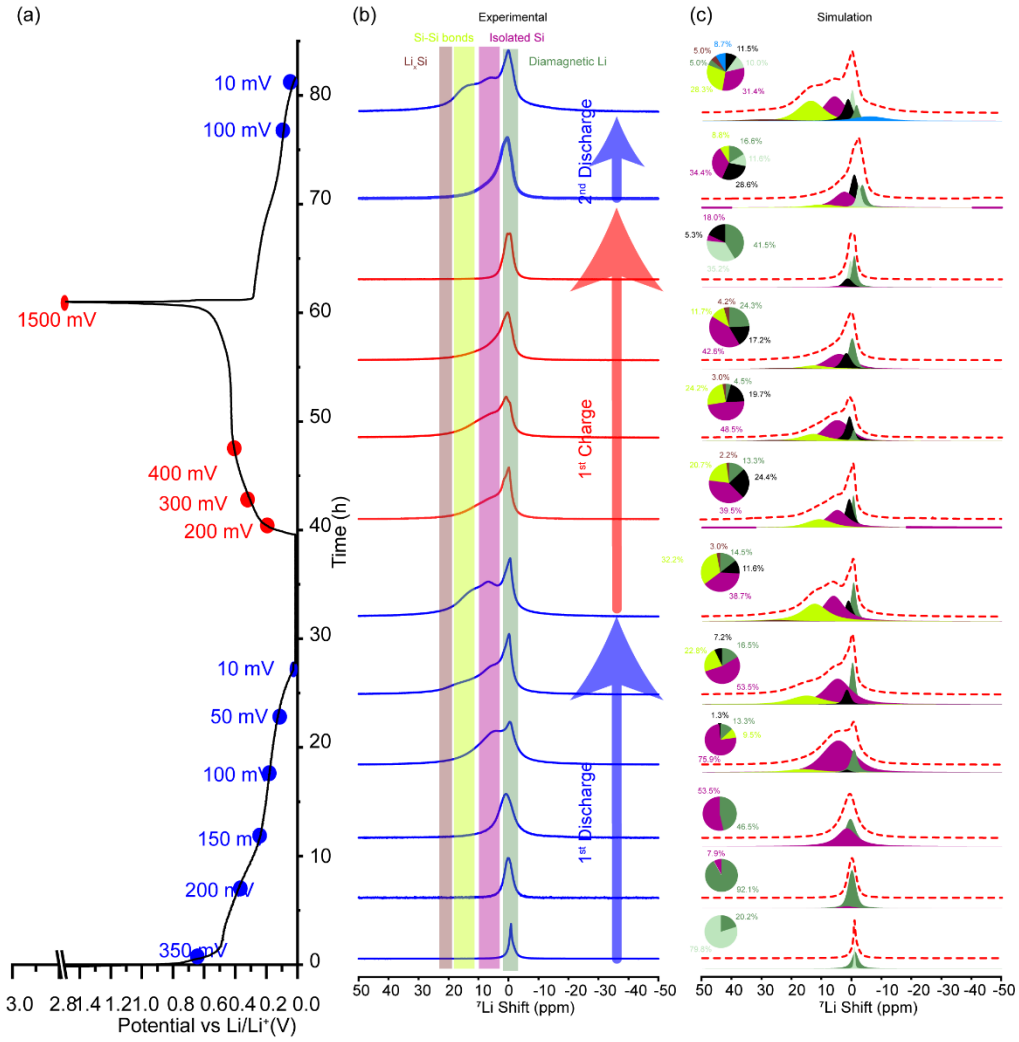

Figure 2. Electrochemistry data (a), *ex-situ* ^{7}Li NMR spectra (b) and the corresponding spectral simulation (c) of GFM series.

High resolution ^{7}Li NMR sheds lights on the local Li environment changes during lithiation/delithiation, however Li NMR signal cannot be distinguished from the numerous Li resonances and it can only indirectly probe the Zintl phase formation. To get a better understanding of what particular Si species formed and how the dynamics changes during cycling, ^{29}Si NMR measurements have been performed on samples collected from pouch cells (cycles against lithium) to increase the signal intensity .Electrochemistry data of both GF and GFM series are shown in Figure 3(a), GF provides slightly higher capacity than GFM, which is consistent with our coin cell data sets. ^{29}Si NMR spectra and simulation of GFM and GF are shown in Figure 3(b) and (c), respectively. Upon discharge, both spectra have a sharp component around -80 ppm, which is assigned to be lithiated SiO (the total content is underestimated to due experiment parameters used). The broad peak resonating at -15 ppm is isolated Si particles. The positive shift around 220 ppm is partially lithiated Si clusters. At 100 mV, the majority reactive Si is isolated Si, which is in great agreement with the ex-situ Li NMR results. At fully lithiated state, both series give one single peak, however GFM one resonates at -25 ppm and GF is about 30 ppm. The shift difference is due to the presence of Li-Mg-Si, this ternary phase would significantly affect the local electron density, leading to a negative chemical shift. Upon charge, a large amount (~47.7%) of partially lithiated Si was observed in GFM sample, compared with only 11.5% residual Si in GF cell, indicating that Zintl phase help stabilize the interaction between SI and Li. Additionally, there is shoulder peak at 440 ppm showing up only in the GFM cell. It is possible that this environment is partially delithiatedMg-Si species formed after Li

removal from the original ternary phase with a composition Li_yMgSi_x where x is low and Mg:Si ratio can be as high as 0.5. Future experiments are needed for accurate determination of these amorphous structural phases

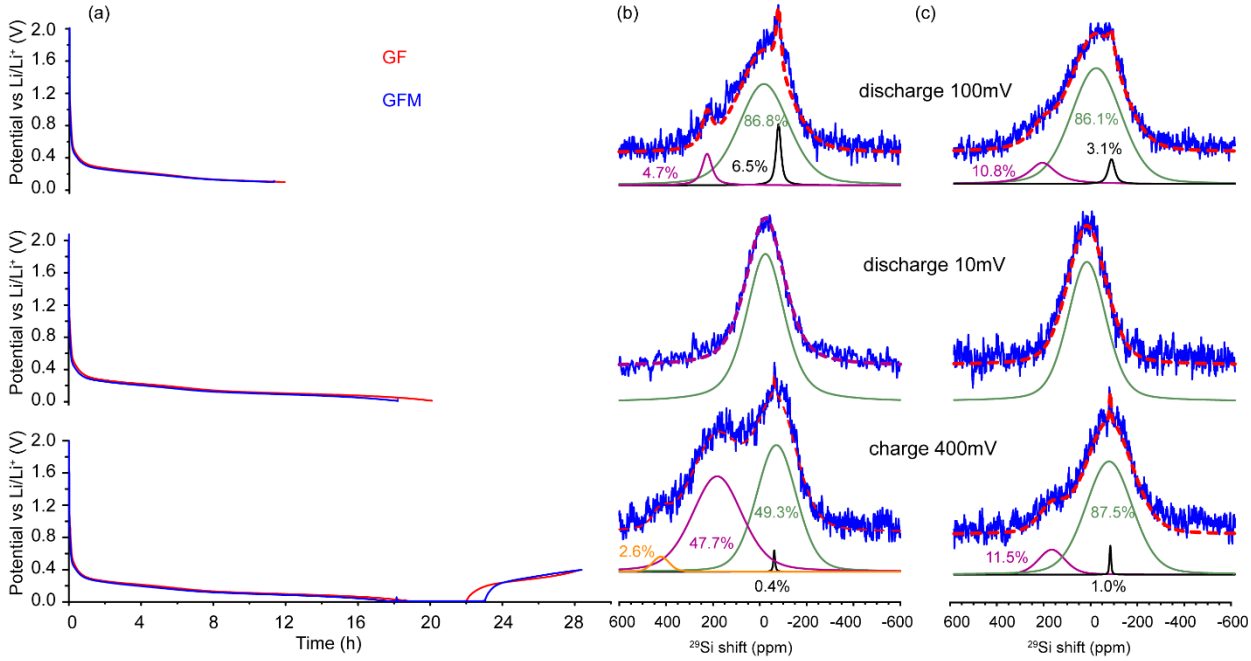

Figure 3. Electrochemistry performance of GF and GFM at 100 mV, 10 mV and 400mV.(a) Experimental data(solid line) and simulation (dash line) of GFM(b) and GF(c).

Conclusions

In this work, we successfully study the formation of local Li and Si environments at different charge states and quantify the Li/Si dynamics upon lithiation/delithiation. The differences in chemical shift, line shape and intensity indicate the formation of Zintl phase at the late state of discharge. Possible mechanism is also proposed: Li-Mg-Si formed in bulk at low potential during discharge and partially delithiated Mg-Si phase remains as Li extracted upon discharge.

References

1.Baran, V., van Wüllen, L. & Fässler, T. F. Substitution of Lithium for Magnesium, Zinc, and Aluminum in $Li_{15}Si_4$: Crystal Structures, Thermodynamic Properties, as well as ^6Li and ^7Li NMR Spectroscopy of $Li_{15}Si_4$ and $Li_{15-x}M_xSi_4$ (M=Mg, Zn, and Al). *Chem. Eur. J.* **22**, 6598–6609 (2016).

2. Zeilinger, M., Benson, D., Häussermann, U. & Fässler, T. F. Single Crystal Growth and Thermodynamic Stability of $Li_{17}Si_4$. *Chem. Mater.* **25**, 1960–1967 (2013).

3. Han, B. *et al.* Using Mixed Salt Electrolytes to Stabilize Silicon Anodes for Lithium-Ion Batteries via in Situ Formation of Li–M–Si Ternaries (M = Mg, Zn, Al, Ca). *ACS Appl. Mater. Interfaces* **11**, 29780–29790 (2019).

4. Key, B. *et al.* Real-Time NMR Investigations of Structural Changes in Silicon Electrodes for Lithium-Ion Batteries. *J. Am. Chem. Soc.* **131**, 9239–9249 (2009).

5. Key, B., Morcrette, M., Tarascon, J.-M. & Grey, C. P. Pair Distribution Function Analysis and Solid State NMR Studies of Silicon Electrodes for Lithium Ion Batteries: Understanding the (De)lithiation Mechanisms. *J. Am. Chem. Soc.* **133**, 503–512 (2011).

6. Michan, A. L., Leskes, M. & Grey, C. P. Voltage Dependent Solid Electrolyte Interphase Formation in Silicon Electrodes: Monitoring the Formation of Organic Decomposition Products. *Chem. Mater.* **28**, 385–398 (2016).

Part 3: Understanding the mechanical properties of the SEI

Calorimetric and Stress Measurement of Model Si electrodes for SEI formation Studies

Josey McBrayer (SNL), Eric Allcorn (SNL), Chris Apblett (SNL), Jill Langendorf (SNL), Teal Harbour (SNL)

Background

Stress and strain evolution are implicated in the long term instability of the SEI due to volumetric expansion and contraction of the Si during lithiation/delithiation events, but SEI evolution due to lithium insertion directly into the SEI, as well as the evolution of the SEI towards inorganic Li2O and other structures, may also play a role in the subsequent electrochemical behavior of both model (2D) and real (3D) Si structures. Measurements that allow for isolation and measurement of these properties provides insight into these evolutionary processes. This work addresses milestone 7.

When processed and incorporated into electrodes, silicon active material surfaces are altered from their pristine conditions in a way that likely influences SEI formation and function. To understand the difference between model silicon systems and powders incorporated into electrodes, microcalorimetry has been employed to measure the heat generated from the aqueous processing of silicon powders with LiPAA binders and carbon additives. This technique provides insight into the formation processes and how they are affected by using binders, something that is not used in the model thin film processes and provides additional fidelity to the real electrode system. This work addresses milestone 2 and milestone 8.

Results

We have made marked progress towards measuring the stress of SEI formation in-situ during electrochemical cycling of thin films. To overcome some of the challenges this measurement presents, new samples needed to be prepared that present a continuous, clean Si substrate to the electrolyte, but provide for very thin structures that are sensitive to changes in geometry so that accurate measurements of stress can be made. An improved sample processing process that utilizes a protective thick oxide layer over the test 50nm silicon surface has allowed for much more aggressive processing of the photoresist release layer, allowing us to use highly energetic oxygen plasmas to remove residues, and then subsequently perform an HF dip to clean off the sacrificial surface oxide, leaving only clean silicon. Electrochemical cycling of samples prepared in this manner have yielded excellent CV curves that mimic those found on thick Si wafers, indicating that the cleaning process is not leaving any electrochemically active residues behind. These samples also have a 2um thick evaporated Cu backing layer, and then a Si moiré fringe pattern deposited on the back side of the Cu foil. This fringe pattern is critical to the accurate measurement of in plane stress and strain of the Cu layer and Si layer exposed to the electrolyte.

Optical improvements for the samples include the use of a new grid pattern that is designed specifically for this work, allowing for an optimal fringe pattern to be used in the right place on every sample. Temperature control and vibration isolation have lowered the noise floor for the imaging of the fringes. A new design for the sample holder that allows for pressure relief, exposure to electrolyte while under moiré imaging, and minimized volumes for electrolyte (now compatible with the volume of a coin cell). All of these improvements have resulted in enough improvement in resolution to begin the measurement in situ of the strained samples directly as the electrolyte is exposed to the Si, and as the sample is cycled to form the SEI. However, additional work is needed, as the measurement from the moiré pattern are not precisely correlated to stress, due to a need to have calibration standards for these measurements. This work is being undertaken now and should result in a direct, calibrated measurement of stress as the electrochemical processes proceed on the thin Si sample. A mosaic showing the processing, hardware fixtures, and moiré camera is shown in Figure 1.

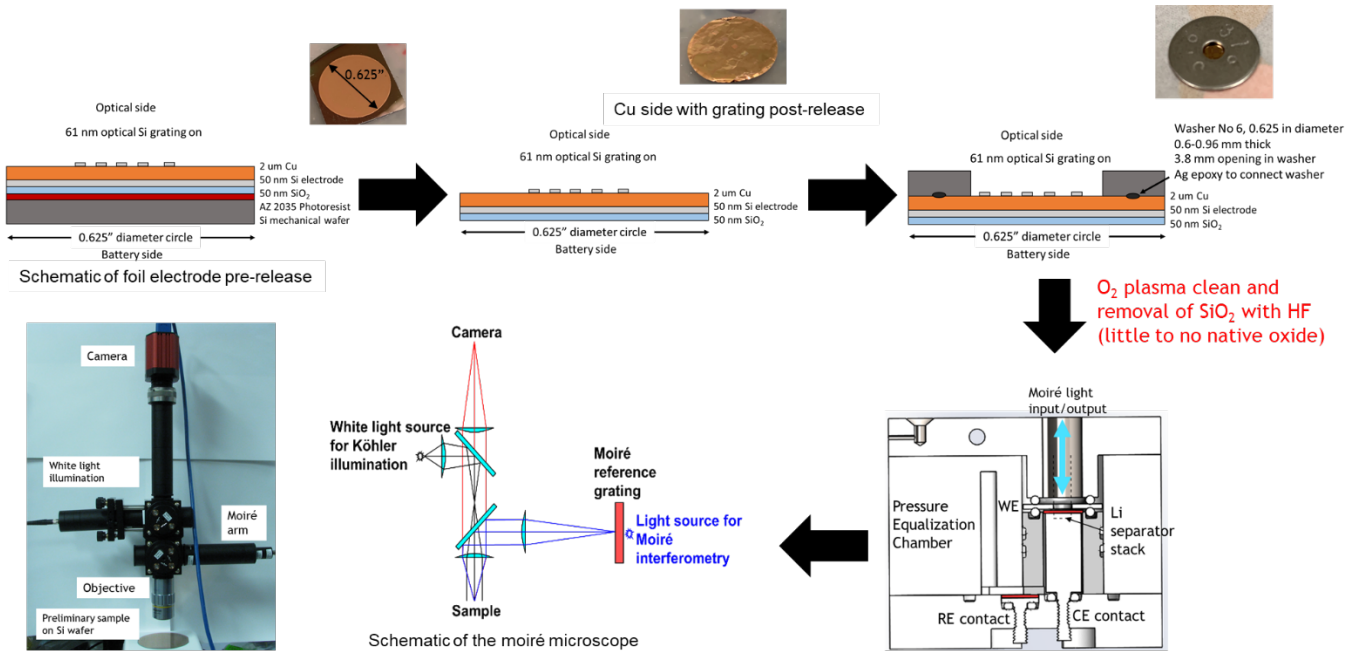

Figure 1. Mosaic of wafer processing to produce samples (upper row), and sample chamber design and moire camera setup.

Because both the electrochemical cycling and the stress measurements are done in situ, comparisons with potential can be made between the electrochemical phenomena and the electrochemical phenomena directly. For the first formation cycle of lithiation and delithiation for preliminary (non-calibrated) results is shown in Figure 2. It should also be noted that this sample was prepared without the protective SiO2 layer and was performed on a thicker Si substrate (150nm), so the standard samples are likely to have different performance. Still, there is clear correlation between the region of voltage prior to the onset of lithiation above 0.5V, and the start of lithation. The film undergoes a slow increase in tensile stress (perhaps due to SEI formation through chemical, rather than electrochemical, processes), and then an abrupt change to compressive film as the Si starts to lithiate. Since the film is a composite of SEI and Si, it is reasonable to assume a compressive stress is expected as the Si expands on lithiation.

On delithiation, the data is more confusing, but a clear drive towards high compressive state (perhaps due to the SEI now dominating the stress response), followed by a return to near neutral stress after the film has been fully delithiated above 1 volt. Since this was done at a single scan rate for potential, it may be that this response is time based, or potential based. Changing sweep rates of these measurements will allow us to differentiate between the two phenomena.

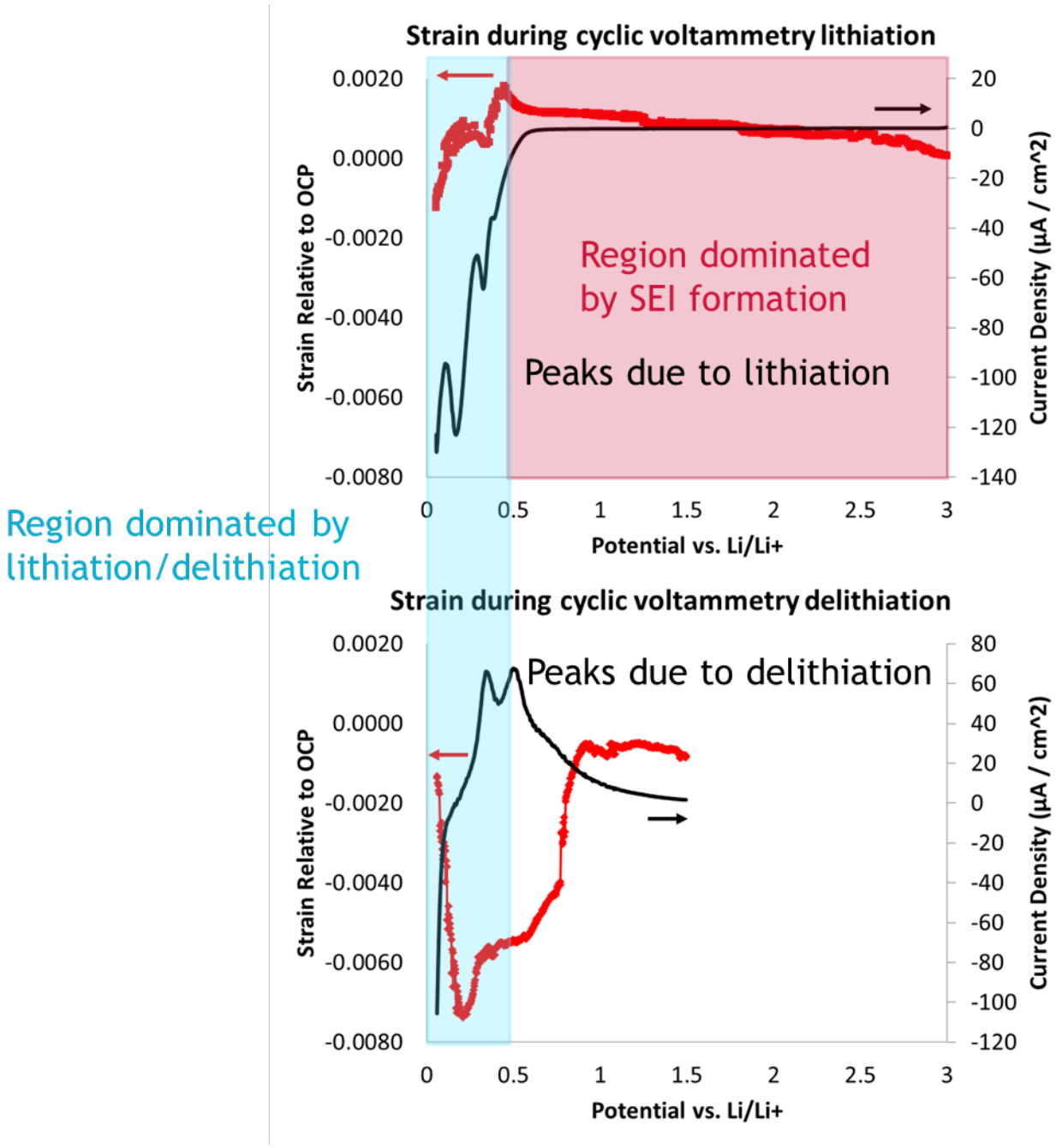

Figure 2: Combined stress and electrochemical measurements on the first cycle of a 150nm thick Si on 2um thick Cu substrate. Stress measurments are performed through moire interferometry. Conditions: 100uV/sec sweep, 25C, CE/RE: Li metal, Electrolyte: 1.2M LiPF6 in 3:7 EC/EMC

With the technique for in situ measurement of stress and electrochemistry established, we will start to investigate the impact of electrolyte additives, electrochemical holds, and film thickness/scan rate for stress behavior in the system, with an intent to understand how these factors impact the overall formation and evolution of the SEI and stress in the films.

Microcalorimetry:
Previous isothermal microcalorimetry curves of nanosilicon from various suppliers showed the Paraclete-4KD material to have one of the highest peak and average heat generation over the test duration, correlated to its high BET surface area. While generated heat was known to correlate to BET surface area, this material sample was noted to also have poor surface properties that impacted cycling performance. We hypothesized that these surface properties may also correlate with our high heat generation. However, similar analysis of new Paraclete-G18 material, with improved surface properties and cycling, demonstrated nearly identical heat generation. This suggests that surface area is the primary correlative property, as both samples showed similar BET surface areas. This data is summarized in Table 1.
Electrochemical microcalorimetry has also been carried out on two silicon containing coin cells. The microcalorimetry fixture was first calibrated for dynamic time correction using a "dummy" coin cell of known resistance to both confirm measurement accuracy and enable reduction of signal latency by roughly one order of magnitude. [1] Figure 3a shows the overlay of the voltage and heat generation curves for a full coin cell of NMC cathode vs Paraclete G18 anode. While the current level of analysis does not enable us to isolate parasitic heat flow from other sources (entropic and ohmic) it does provide quantification of the overall reduction in heat generation with subsequent cycling. [2] Figure 3b shows the measured coin cell capacity along with heat generated per cycle, with both showing similar decreasing trends. The values measured here also agree closely with those reported in a newly accepted paper on microcalorimetry of silicon anodes. [3] Continued electrochemical microcalorimetry testing of coin cells will enable comparison of heat generation between cathodes and anodes within cells and, through controlled discharge parameters, enable isolation of the parasitic heat flow from the entropic and ohmic heat flow coming out of the tested coin cell. This will enable us to determine the point of cycling with peak parasitic losses as well as, though charge counting potentiostatic measurements, determine the heats of formation for SEI layers at different states of charge.

Table-1: The quantified energy generation based on the fit curve of the Paraclete-4KD + CB sample in Figure 1 as well as predicted material and performance loss based on the formation of silica.

	Peak Signal, uW	Average Signal, uW	Normalized Peak Signal, uW/g-Si	Normaled Peak Signal, uW/m²-Si
90.7	90.7	64.2	468.6	13.9
Paraclete G18	97	57.3	489	15.2

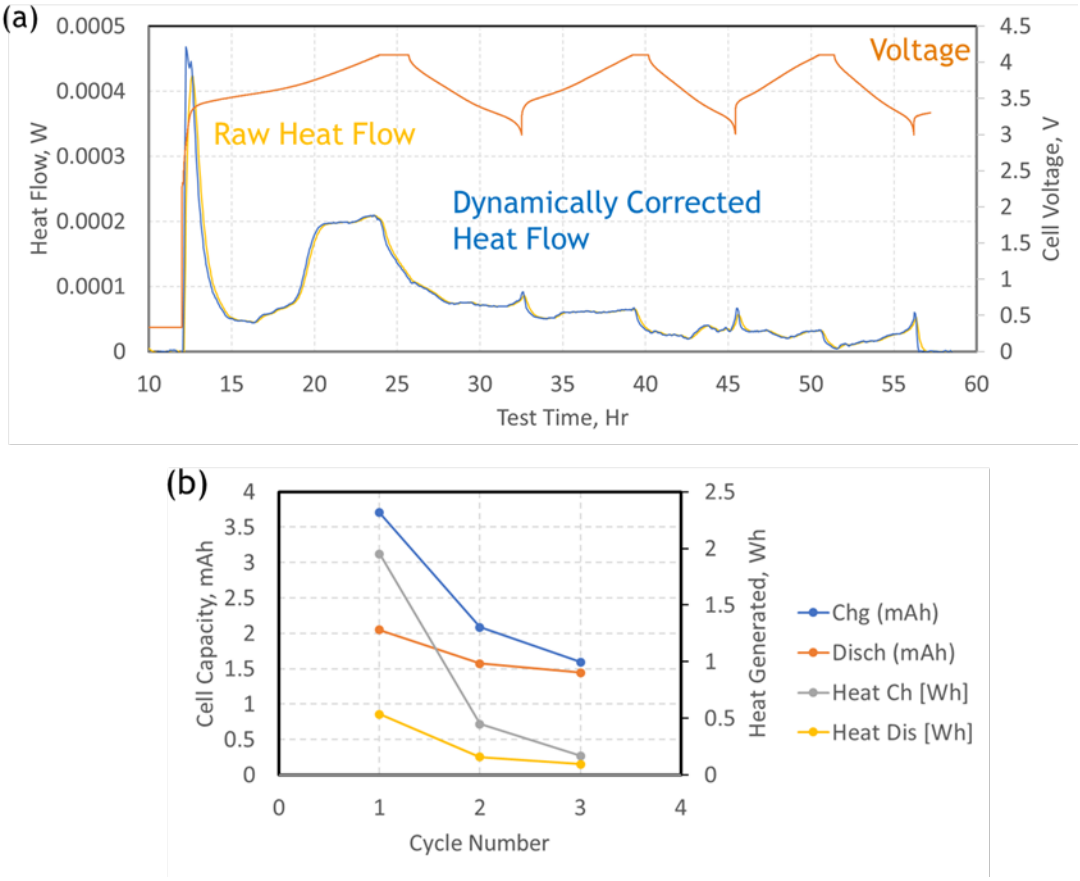

Figure 3: a) Heat flow and voltage curves for NMC vs Paraclete-G18 coin cell subjected to electrochemical microcalorimetry. b) The cell capacities and generated heat per cycle derived from these curves.

Conclusions

We have demonstrated both the capability to perform simultaneous measurement of stress and electrochemical behavior in situ in a test system with appropriate levels of electrolyte present in the system. The preliminary results from this technique seem to agree with what is to be expected from early observations of SEI formation; that of slow formation of chemical effects above the lithiation potential, followed by rapid evolution of compressive stress as the Si lithiates. On delithiation, the film continues to be compressive (which may indicate a change in dominant stress behavior), followed by a return to neutral stress state above the lithation potential. Microcalorimetry has been used to make comparisons between two of the Paraclete films, and has shown that the amount of parasitic (perhaps associated with SEI formation) heat generation is cycle dependent, and is reduced with cycling, suggesting that these systems are coming to an equilibrium state after a few cycles.

References

1. S.L. Randzio, J. Suurkuusk, A.E. Beezer (Ed.). *Biological Microcalorimetry,* Academic Press (1980), pp. 311-341.
2. L. J. Krause, L. D. Jensen, J. R. Dahn. *J. Electrochem. Soc.* **159** (2012) A937-A943.
3. L. M. Housel et. al. *ACS Appl. Mater. & Interfaces* ***Just accepted*** (2019).

Decoupling electrochemical and mechanical instabilities of SEI upon cycling (LBNL)

Elisabetta Arca, Insun Yoon, Terri Lin, Philip Ross, Robert Kostecki (LBNL)

Background

The low coulombic efficiency of Si-based anode is a well-known problem, caused by the instability of the SEI over cycling. Two major sources of the instability are suggested to originate from (i) the inherent chemical or electrochemical non-passivating behavior and (ii) Si volume change-induced mechanical deformation. We developed two experimental model approaches in order to decouple the contributions from the two sources to the cycling inefficiency.

To unravel the cause of the (electro)chemical instability, we analyzed the composition of the SEI after the first half and full cycle as well as after the second half and full cycles by means of X-Ray Photoelectron Spectroscopy (XPS). Specifically, we run a quantitative analysis on the SEI components to distinguish between the products formed as a result of the salt and solvents decompositions respectively. This helps to determine which reaction is not getting suppressed after the SEI formation, thus causing continuous electrolyte decomposition.

To investigate the quantitative influence of the mechanical degradation of SEI, we designed the following comparative study: A test sample allows lateral expansion of Si thin film electrode by using a polymeric substrate (polydimethylsiloxane – PDMS), while a control sample does not allow the lateral expansion by using a rigid substrate (fused silica). The lateral expansion of Si thin-film electrodes directly translates to mechanical stretching of SEI, i.e., the SEI formed on the test sample is expected to undergo mechanical deformation while that formed on the control sample does not. Comparing the cycling performance and the SEI compositions of the two types of samples is expected to unveil the influence of the mechanical deformation effect. As the first step, we conducted preliminary experiments to establish a proof of concept of this approach.

Both studies contribute to a comprehensive understanding of the decomposition reactions at the Si-electrolyte interface. The results using the conventional Gen II electrolyte can provide a strong base-line. Furthermore, the developed experimental systems can be extended to other electrolyte compositions containing solvents or additives or different electrode formulations (Zntil phases or Si-metal alloys).

Results

In order to study the composition of the SEI as a function of state of charge and cycle number, the a-Si/n-SiOx thin films were galvanostatically cycled, rinsed and transferred into the XPS system through air-tight systems. For each sample, XPS spectra were acquired and peaks were fitting in order to determine the species present and their relative concentration. An example of the fitting procedure for some relevant core levels is shown in Figure 1 whereas the results of the quantitative analysis are shown in Figure 2.

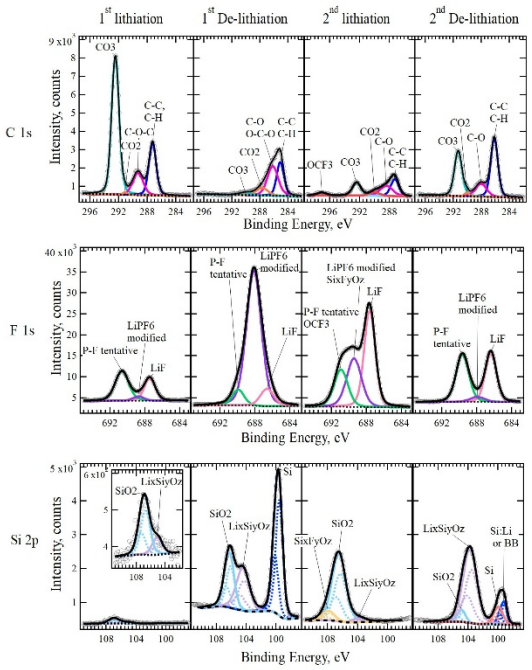

Figure 1. An example of the fitting routine used for the phase identification applied to the C 1s, F1s and Si2p core levels.

Upon the first lithiation, the SEI is rich in the decomposition product of the solvent (overall C signal is ~20 at.%, of which 10 at.% is due to carbonate alone). The salt-derived decomposition products are far less, about 10 at.% based on fluorine, of which only a small fraction (~2 at.%) is due to LiF.
Upon delithiation, the composition of the SEI changes drastically. The amount of carbonate species after delithiation is extremely low (0.4 at. % based on C), a reduction by a factor of 30 with respect to the carbonate content present in lithiation stage. Surprisingly, the decomposition product of $LiPF_6$ is the major inorganic component, whereas LiF does not vary by much in comparison to the previous measurements.
During the second lithiation, the SEI forms again but with a composition different than the one formed during the first lithiation. Carbonate is the main C-containing species but they are present in a much lower concentration (1.36 at. % in the second lithiation vs. 11.6 at. % for the first lithiation, thus about an order of magnitude lower). This means that the surface has been largely passivated with respect to the decomposition of the organic solvents and only a tenth of the decomposition of the organic solvent is still happening during the second lithiation. Conversely, the amount of salt-decomposition products is still quite considerable. Indeed, LiF is the major SEI component formed during the second lithiation, with a relative at.% 4-5 times higher than in previous samples (first lithiation and first delithiation). Finally, during the second delithiation, the SEI dissolves or detaches again. LiF is still the main component of the SEI, although its at.% is lower than before. Carbonate is present too but in much lower quantities with respect to fluorinated compounds.

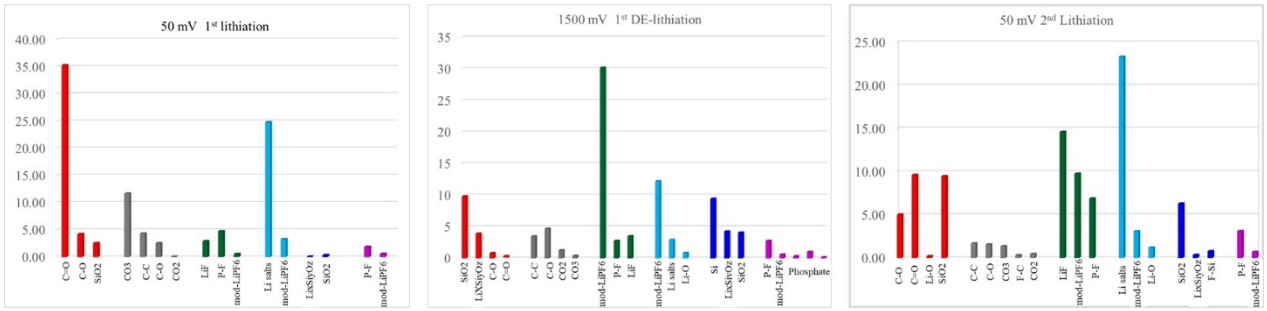

Figure 2. XPS quantitative analysis shown for the first lithiation, first delithiation and second lithiation process.

In regards to the experiments on the mechanical instability of SEI, the lateral expansion of the Si electrode on the polymer substrate (test sample) appears in the form of surface wrinkling. A mechanics analysis suggests that the wrinkles have a uniform wavelength to minimize the total strain energy [1]. Thus, the amplitude and the wavelength of the wrinkles can provide a quantitative level of SEI stretching. Figure 3 summarizes the results from our preliminary experiments where we observed this phenomenon. First, a thin film electrode consisting of Ti(~10nm)/Ni(~50nm) current collecting layer and Si(~60-70nm) layer was created by sputter deposited on a PDMS substrate (Figure 3a). Second, we designed/fabricated a custom electrochemical cell for in situ optical microscopy (Figure 3b). The sample was assembled to the custom cell and integrated into an optical microscope (OM) setup. Next, the Si thin film electrode was electrochemically cycled while the OM captured the surface topography evolution in real-time. Figures 3c-e show three representative OM images taken at as-prepared, lithiated, and delithiated state of the Si electrode, respectively. Also shown is the two-dimensional (2-D) fast Fourier transform (FFT) images which visualizes the characteristics of the wrinkled patterns. The electrode was initially flat without any pre-wrinkles; thus, the corresponding FFT image shows no particular pattern (Figure 3c). After the first lithiation, the lateral expansion of Si spontaneously formed surface wrinkling (Figure 3d). Distinctive high-power location was observed in the FFT image (highlighted in dashed squares); this indicated that there was a characteristic wavelength of the wrinkles of which was approximately 24 μm. The wrinkles mostly disappeared after the subsequent delithiation due to the contraction of the Si electrode (Figure 3e). A minor wrinkled patter may be attributed to irreversible Si volume change. The corresponding FFT image also showed a drastic decrease of power which confirms the fading of the wrinkles. This series of observations implied that the thin-film electrode on a polymer substrate can apply cyclic strain on the SEI.

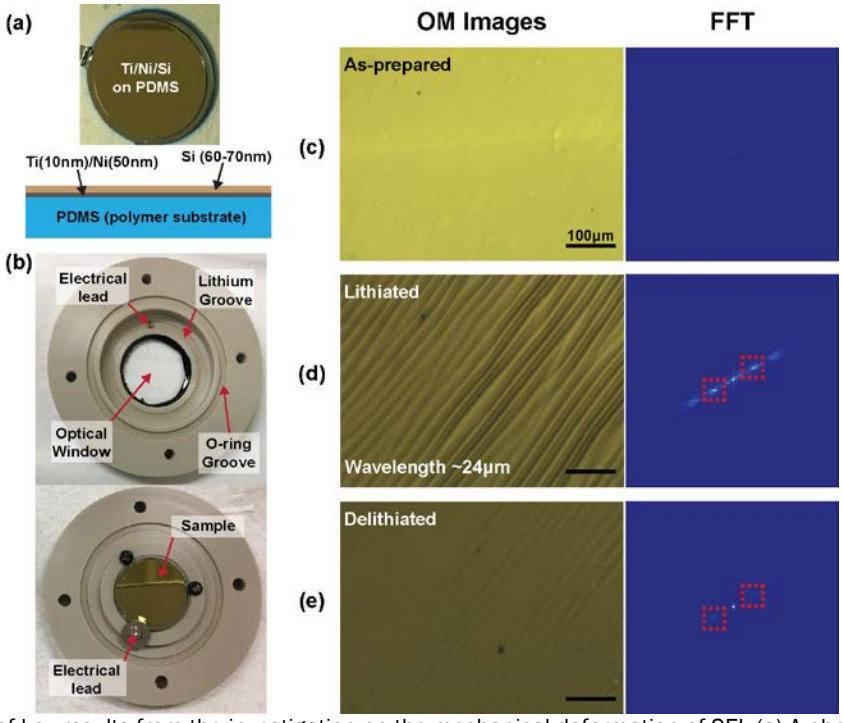

Figure 3. Summary of key results from the investigation on the mechanical deformation of SEI. (a) A photograph of Si thin film electrode consisting of Ti(10nm)/Ni(50nm)/Si(60-70nm) layers on a PDMS substrate. Also shown is a schematic of illustration of the electrode structure. (b) A photograph of a custom electrochemical cell for in situ optical microscopy (OM). (c-d) OM images of the sample surface at as-prepared, lithiated, and delithiated states. Also shown are corresponding 2-D FFT images.

Conclusions

Two model experimental systems have been developed to decouple the effect of the (electro)chemical processes versus the instability induced by the mechanical processes as a funciton of states of charge and number of cycles.
To assess the former, we performed a quantitative analysis of the insoluble components forming the SEI. We determine that the reduced rate of decomposition of the organic solvents present in the electrolyte is responsible for the higher coulombic efficiency during the second electrochemical cycle in comparison to the first, whereas the rate of salt decomposition and reactivity of this toward the electrode is almost unchanged between cycles.
To assess the latter, we designed an experimental platform that can stretch/unstretch the SEI layer utilizing the Si volume change. The results from in situ OM experiments show a spontaneous formation and the disappearance of surface wrinkles during lithiation and delithiation of the Si electrode on the soft substrate. These results from the preliminary experiments provide proof of the concept of our approach. Further improvement of the approach is expected to reveal the quantitative influence of the mechanical degradation of SEI on the cycling performance of Si anodes.

References

[1] Huang, Z.Y.; Hong, W.; Suo, Z. J. Mech. Phys. Solids 53 (9), 2101-2118 (2005)

Part 3: Understanding the chemical properties of the SEI

Influence of CO_2 on the stability of a Si SEI

Gabriel M. Veith, Emma J. Hopkins (ORNL); Nate Neale, Ryan Pekarek (NREL) Gao Liu (LBNL)

Background

There have been several reports of carbon dioxide gas providing a beneficial role in SEI formation and stabilization.[1-4] Within this new task we are seeking to reproduce and understand this effect. To accomplish this the team is working to construct a set of experiments on a common set of materials. ORNL is preparing the thin film electrodes, forming pouch cells, and cycling the materials. After cycling team members will analyze parts of the resulting SEI chemistry with techniques specialized to their facilities. This includes FTIR and XPS (NREL), SEI solubility (LBNL), Raman (ORNL) and other characterizations.

Results

In this quarter the team has developed the architecture needed to support these experiments. Thin silicon films were deposited on 2" by 2" copper foils with a copper tab, Figure 1-left. A lithium counter electrode was created (Figure 1 – center left). The electrodes were assembled into a pouch cell (Figure 1-center right) and injected with carbon dioxide (Figure 1-right). The experimental plan involves cycling these batteries to 0.05V one and ten cycles and evaluating the coulombic efficiency and differences in the SEI chemistry.

Figure 1. Images of the Si electrode (left), Li electrode (center left), pouch cell being injected with electrolyte (center right) and pouch cell injected with CO_2 (right).

Figure 2 shows representative cycling data measured for the first lithiation process. The cells are cycled at a rate of C/10. After delithiating to 0.3 V the cell was disassembled and washed using 5 mL of dimethyl carbonate. The resulting electrode is a homogenous black (Figure 2 top right) indicating homogenous lithiation. Note prior experience shows inhomogeneous lithation results in a multicolored electrode surface. The electrode was sectioned and shipped to partner laboratories for evaluation.

Preliminary C1s, P2p and F1s XPS data are show on the bottom of Figure 2, respectively. From this data it is clear that there are significant changes in the SEI chemistry with and without CO_2. Preliminary quantitative analysis indicates that the cell with CO_2 has higher concentrations of C-C and CO_3 type functionality (C1s data). Furthermore, the P2p and F1s data indicates the CO_2 promotes the decomposition of the $LiPF_6$ salt resulting in more POF type species.

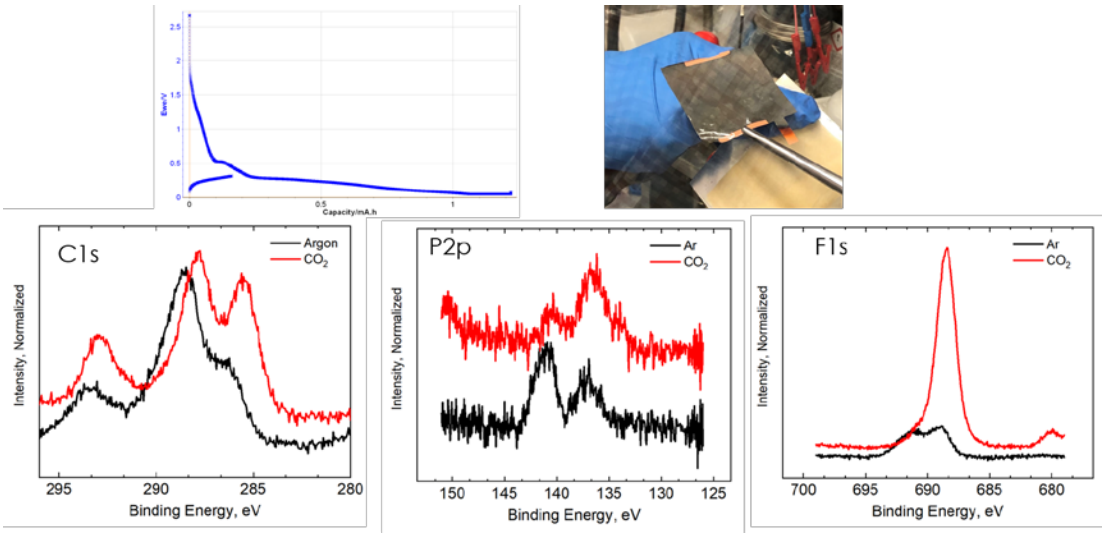

Figure 2. Top Left – Cycling data for a representative electrode; Top Right – Image of a lithiated electrode; Bottom row – C1s, P2p and F1s XPS data collected for cells cycled in argon or CO_2 atmospheres.

Conclusions

From the data presented we have developed an architecture to explore the role of CO_2 on SEI formation and are seeing clear preliminary evidence that the SEI chemistry varies significantly with CO_2. Cycling continues to explore the SEI and cycling efficiency with time. One challenge is to identify if the CO_2 aids just the Si or the Li counter electrode as well.

References

1. Sawa, S.; Minami, H.; Torimae, M.; Fukui, A.; Kusumoto, Y.; Sayama, K.; Kamino, M. Lithium secondary battery including a negative electrode which is a sintered layer of silicon particles and/or silicon alloy particles and a nonaqueous electrolyte containing carbon dixoide dissolved therein and method for producing same. 2012.

2. Krause, L. J.; Chevrier, V. L.; Jensen, L. D.; Brandt, T., The Effect of Carbon Dioxide on the Cycle Life and Electrolyte Stability of Li-Ion Full Cells Containing Silicon Alloy. *Journal of The Electrochemical Society* **2017,** *164*, A2527-A2533.

3. Chevrier, V. L.; Krause, L. J.; Jensen, L. D.; Huynh, C.; Triemert, M.; Bowen, E. L.; Thorson, J., Design of Positive Electrodes for Li-Ion Full Cells with Silicon. *Journal of The Electrochemical Society* **2018,** *165*, A2968-A2977.

4. Solchenbach, S.; Wetjen, M.; Pritzl, D.; Schwenke, K. U.; Gasteiger, H. A., Lithium Oxalate as Capacity and Cycle-Life Enhancer in LNMO/Graphite and LNMO/SiG Full Cells. *Journal of The Electrochemical Society* **2018,** *165*, A512-A524.

Computational Determination of the Silicon Electrolyte Interface.

Kristin Person University of California Berkeley

The self-diffusion coefficients of the EC (1.2 M $LiPF_6$ in EC), ECF (1.2 M $LiPF_6$ in EC w/ 10% FEC), Gen2 (1.2 M Li in EC:EMC (v/v 3:7)), and GenF (1.2 M Li in EC:EMC (v/v 3:7) w/ 10% FEC) electrolytes are calculated using the mean square displacement in the molecular dynamics (MD) simulations. Figure 1 shows

the self-diffusion coefficients of each species (EC, EMC, FEC, PF_6^-, and L^{i+}) in the four model electrolytes. Comparing to the EC/ECF electrolyte, the Gen2/GenF electrolyte exhibits a higher self-diffusion coefficient for each species, due to the addition of the less viscous linear carbonate (EMC). Meanwhile, the addition of FEC does not significantly influence to the diffusivity of the EC or Gen2 electrolytes.

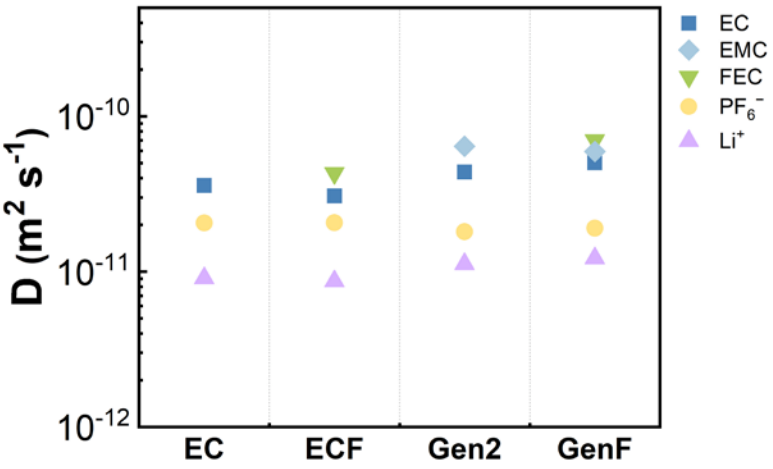

Figure 1. Self-diffusion coefficients of electrolyte species (EC, EMC, FEC, PF_6^-, and Li^+) in the EC, ECF, Gen2, and GenF electrolytes.

In order to study the difference in conduction mechanism between the EC and Gen2 electrolyte, the trajectory of Li-PF_6 coordination are sampled from the MD simulation. Figure 2 shows two representative Li-PF_6 coordination distance as a function of time in a) EC electrolyte, and b) Gen2 electrolyte, respectively. It can be noted that the Li^+ in Gen2 electrolyte spends a larger proportion of time coordinated to PF_6^-, indicating that in Gen2 electrolyte, Li travels longer in time with PF_6^-.

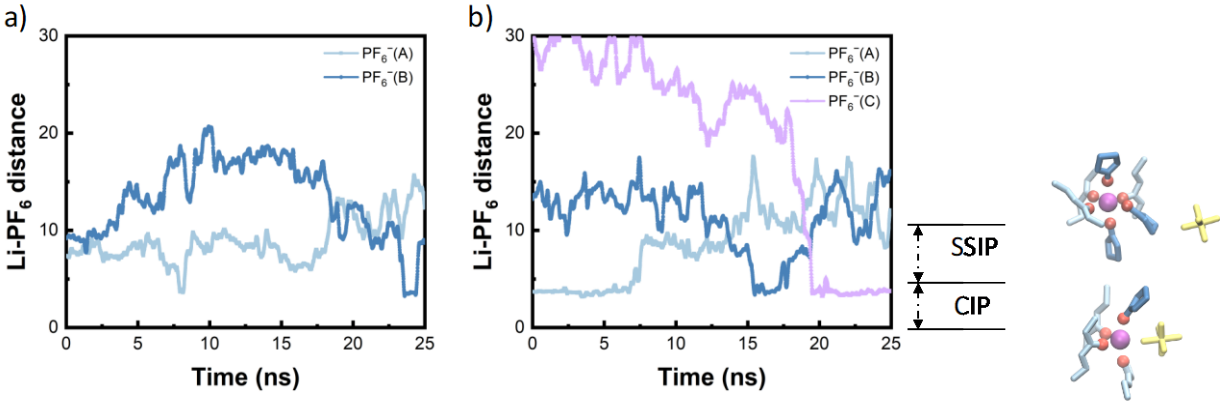

Figure 2. The representative trajectory of Li-PF_6 coordination distance as a function of time in a) EC electrolyte, and b) Gen2 electrolyte. A cutoff distance of 5 Å is used to differentiate contact ion pairs (CIP) and solvent separated ion pairs (SSIP).

Si electrode performance, including volumetric expansion, voltage, and diffusivity, may be improved through the use of additive elements or alloying. Volumetric expansion is a crucial factor in cycling stability of an electrodes. Obrovac et al. previously asserted that the volumetric expansion of Si upon lithiation is linearly proportional to the number of Li atoms inserted, 14.8 $Å^3$ per Li atom.[1] This assertion, however, assumes that

the linear relationship between volume and # of Li alloyed in the crystalline phases applies to the amorphous phases. Here, we present a brief study of the volume change of various amorphous alloy electrodes.

In Figure 3a, we show the evolution of molar volume for the lithiation of a number of elements. It is clearly seen for all elements, except Ca, that there is a favorable interaction with lithium, decreasing the molar volume, in contradiction with Obrovac's assertion. This is more clearly seen in Figure 3b, where the Li partial molar volume changes as a function of the Li concentration, ranging between 15 $Å^3$ and 21$Å^3$ per Li atom. With its consistently high Li partial molar volume (~20.5 $Å^3$ per Li atom), Ca would not be ideal for a low volumetric expansion electrode. Sb exhibits a lower Li partial molar volume than Si, resulting in a lower volumetric expansion 135% at x_{Li} = 0.75 (as compared to ~320% at x_{Li}=0.75 for Si). However, its high initial molar volume is detrimental to its volumetric capacity. Similarly, the addition of elements, such as Ni, to Si affects the molar volume and decreases the Li partial molar volume, dependent on the amount added.

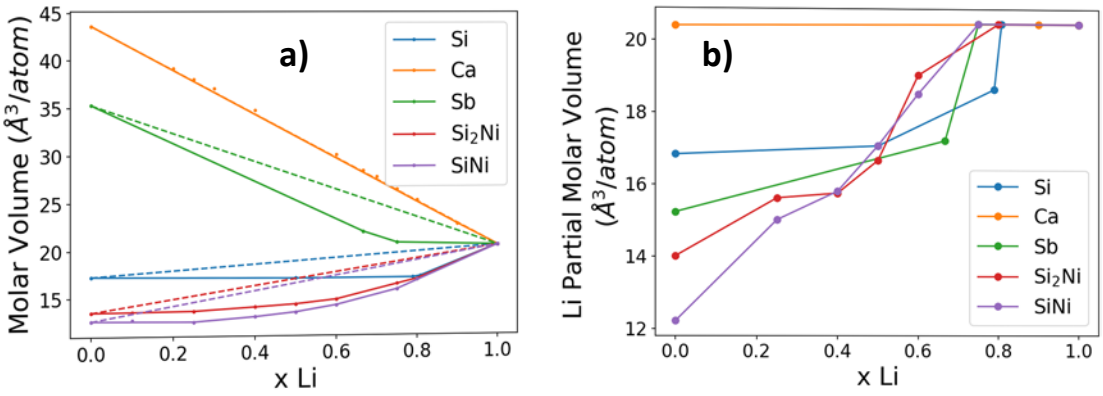

Figure 3. a) Molar volumes and b) Li partial molar volumes of elemental electrodes. The dotted lines in a) indicate the volume of ideal mixtures.

Conclusions

The Gen2/GenF electrolytes are less viscous than EC/ECF electrolytes due to the addition of linear carbonates, while the 10% FEC additive has insignificant influence on the diffusivity. In Gen2 electrolyte, Li travels longer in time with PF_6^-, which is likely to impact interfacial speciation and hence reactivity.

The relationship between Li concentration and volume in the amorphous phases follow a different trend than for crystalline materials, suggesting the choice of active element(s) has an impact on the volumetric expansion and capacity. While small in most cases, this partial molar volume change can provide an avenue for tailored performance, particularly when designing binary or ternary alloy electrodes.

References

1. Obrovac, M. N., Christensen, L., Le, D. B. & Dahn, J. R. Alloy design for lithium-ion battery anodes. J. Electrochem. Soc. 154, 849–855 (2007).

Glyme based electrolytes on model silicon electrodes – SEI composition and morphology

Guang Yang, Gabriel Veith, and Jagjit Nanda (ORNL)

Background

Studies within SEISta team confirm that GenII carbonate-based electrolytes do not effectively passivate silicon surfaces unlike conventional graphite anodes. Controlled corrosion experiments showed a small but finite parasitic or leakage current as a-Si is continuously cycled. One plausible explanation for this could be due to the uninhibited reaction between electrolyte and freshly exposed silicon surfaces since the SEI layer continuously breaks due to large volume changes. One approach to address this issue is to explore solvents and salts other than GenII electrolytes that could potentially demonstrate better passivating properties specifically during early electrochemical cycles. A series of glyme-based electrolytes are thus being explored for their effects on the SEI formation using a model a-Si thin film anode at ORNL. As reported in previous quarter, glyme electrolyte containing lithium bis (fluorosulfonyl) imide LiFSI-DME, and a fluoroadditive, 1,1,2,2-tetrafluoroethyl-2,2,3,3-tetrafluoropropyl ether (TTE) demonstrate better stability on a-Si thin film during extended galvanostatic cycling (GC). At 1C equivalent rate GC test, the capacity retention for GenII in first 110 GC cycles was around 30%, whereas this value of the glyme electrolyte reached close to 89%. Preliminary characterization based on IR spectroscopy indicate that the SEI on a-Si surface possibly has rich polymeric ether-based species. However, chemical details of thus-formed SEI and the role the polymeric ethers to stabilize the a-Si anode still remains largely elusive. In this quarter we report investigation on SEI composition and morphology on cycled a-Si using energy dispersion energy-dispersive X-ray spectroscopy (EDX) and X-ray photoelectron spectroscopy (XPS). Further, the topography of the a-Si cycled in different electrolytes are evaluated by the Scanning Electron Microscopy (SEM).

Results

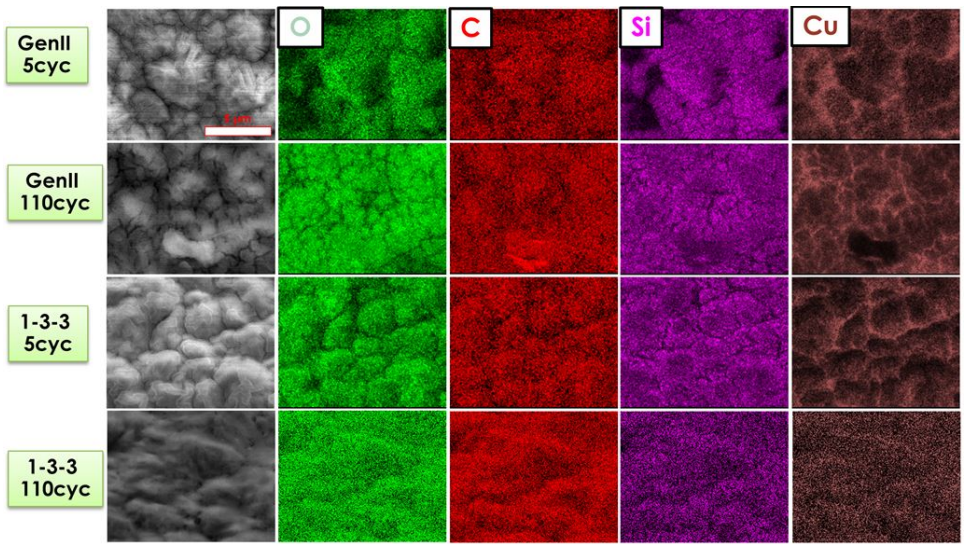

Figure 1. SEM micrographs (left-most column) of cycled a-Si in different electrolytes for various cycle numbers. The EDX mapping of several elements on the corresponding scanned area by SEM are shown on right columns.

Here GenII electrolyte was used as a benchmark. The surface morphology of both early-stage cycling (denoted as 5 cycles) and prolonged cycling (110 cycles) are of interest. For the first 5 cycles, a-Si cycled in both GenII and 1-3-3 (LiFSI-DME-TTE molar ratio as 1:3:3) electrolytes exhibits cracks on the SEI, as shown by both the SEI micrographs and the EDX mapping of oxygen and carbon in Figure 1. Further investigation on the EDX mapping of Si shows that those cracks may stem from the volumetric change of the a-Si thin film upon

(de)lithiation. The EDX mapping of the Cu substrate provides complementary proof towards this point. After prolonged GC, a-Si in GenII electrolyte exhibits more distinguished crack patent, as demonstrated by both the SEM micrographs and the O and Si EDX mappings. In sharp contrast, a crack-free surface was observed for a-Si anode cycled in 1-3-3 glyme electrolyte. Benefiting from this, the surface SEI seems to be more homogeneous and conformal with 1-3-3 glyme electrolyte, as reflected by the O and C EDX mapping in Figure 1. A more conformal SEI on a-Si in 1-3-3 glyme electrolyte benefits better capacity retention.

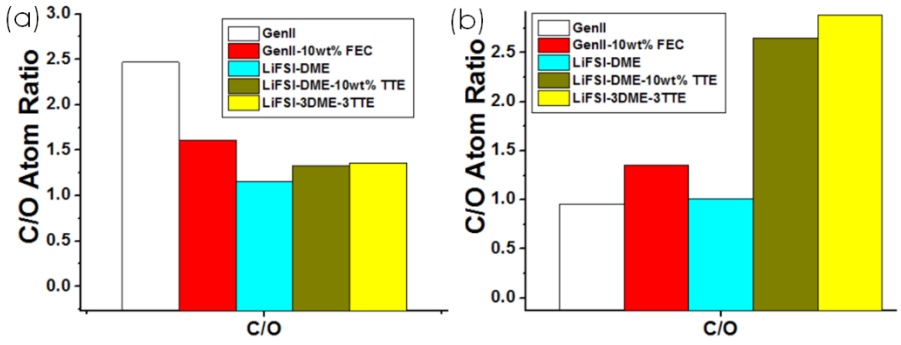

Figure 2. The elemental molar ratio of the C/O analyzed based on the EDX mapping on a-Si anodes for various electrolytes after (a) 5 cycles and (b) 110 cycles.

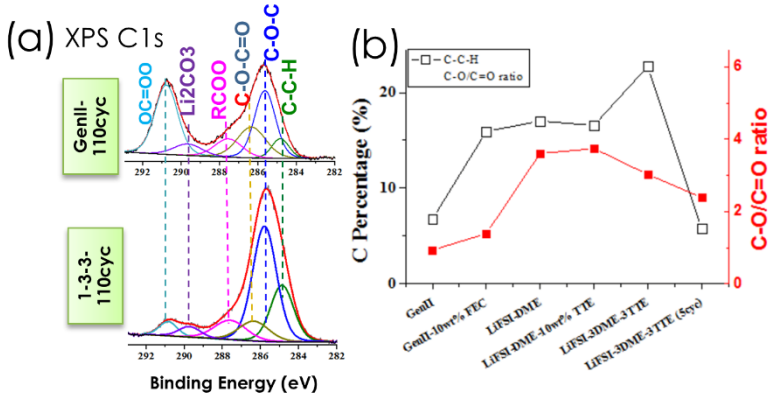

Figure 3. (a) C 1s XPS spectra of the a-Si anodes cycled for 110 cycles in GenII and 1-3-3 glyme electrolytes. (b) The concentration of the C—C-H and the molar ratio of the C-O/C=O for various electrolytes.

The C/O ratio is important because two main polymeric species in SEI, namely polymeric carbonate (-COO) and polymeric ether (-COC) have different C/O ratios. This ratio servers as an initial indication of the concentrations of the carbonate and ether functional groups. Seen from Figure 2, a-Si in GenII electrolytes exhibits high C/O ratio in the early GC stage, whereas the C/O ratio of the a-Si anodes cycled in glyme electrolytes with TTE additive outperforms those cycled in carbonate electrolytes, indicating the increase of the polymeric ether species in SEI. EDX however is relatively bulk sensitive therefore, to determine the surface SEI composition, XPS measurements were performed on a-Si cycled in different electrolytes (Figure 3). It is manifest from the C 1s core level XPS spectra after prolonged GC cycling, ether carbon dominates over other species in the SEI with 1-3-3- glyme electrolyte. In contrast, the SEI of the a-Si anode from GenII electrolyte enriches in carbonate species. The C-O/C=O on a-Si surface with the 1-3-3 glyme is 3.2 times that with GenII electrolyte. The aliphatic chains (C-C-H) has the highest concentration for a-Si with 1-3-3 glyme electrolyte at 22.8%, whereas it was only 6.7% for a-Si cycled in GenII electrolyte. Taken together, the SEI on a-Si anode with 1-3-3 glyme electrolyte has rich polymeric ether species, which are, quite possibly poly (ethylene oxide) (PEO) oligomers. It is also interesting to notice that, at early GC stage (5 cycle), the abundance of the ether function

group is low on a-Si with 1-3-3 glyme electrolyte, agreeing very well with the EDX analysis in Figure 2. It also corresponds to the observation that when cycled in glyme electrolytes, a-Si anode was much less stable due to the large parasitic current (corrosion test using LBNL's protocol shown in a previous quarterly report) compared with GenII electrolyte.

Conclusions

Our studies indicate that when cycled in glyme electrolytes, a-Si model anode has enriched polymeric ether species as one of the primary components of SEI, whereas the GenII counterpart show more polymeric carbonate species. The increased abundance of the polyether rich species could result in a more conformal coating on a-Si anode reliving the local stress and cracks as a result of prolonged electrochemical cycling. This in turn, could result in better stabilization of and enhanced performance. The findings have important implication on investigating alternate electrolytes for high capacity silicon anodes or other metal alloy anodes.